

Introduction of a Methyl Group Curbs Metabolism of Pyrido[3,4-*d*]pyrimidine Monopolar Spindle 1 (MPS1) Inhibitors and Enables the Discovery of the Phase 1 Clinical Candidate *N*²-(2-Ethoxy-4-(4-methyl-4*H*-1,2,4-triazol-3-yl)phenyl)-6-methyl-*N*⁸-neopentylpyrido[3,4-*d*]pyrimidine-2,8-diamine (BOS172722)

Hannah L. Woodward,[†] Paolo Innocenti,[†] Kwai-Ming J. Cheung,[†] Angela Hayes,[†] Jennie Roberts,[†] Alan T. Henley,[†] Amir Faisal,^{†,‡} Grace Wing-Yan Mak,[†] Gary Box,[†] Isaac M. Westwood,^{†,‡} Nora Cronin,[‡] Michael Carter,[†] Melanie Valenti,[†] Alexis De Haven Brandon,[†] Lisa O'Fee,[†] Harry Saville,[†] Jessica Schmitt,[†] Rosemary Burke,[†] Fabio Broccatelli,[†] Rob L. M. van Montfort,^{†,‡} Florence I. Raynaud,[†] Suzanne A. Eccles,[†] Spiros Linardopoulos,^{†,§} Julian Blagg,^{†,§} and Swen Hoelder^{*,†,§}

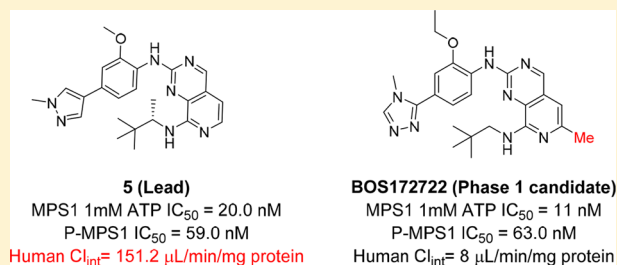
[†]Cancer Research UK Cancer Therapeutics Unit at The Institute of Cancer Research, London SM2 5NG, United Kingdom

[‡]Division of Structural Biology, The Institute of Cancer Research, London SW3 6JB, United Kingdom

[§]The Breakthrough Breast Cancer Research Centre, Division of Breast Cancer Research, The Institute of Cancer Research, London SW3 6JB, United Kingdom

Supporting Information

ABSTRACT: Monopolar spindle 1 (MPS1) occupies a central role in mitosis and is one of the main components of the spindle assembly checkpoint. The MPS1 kinase is an attractive cancer target, and herein, we report the discovery of the clinical candidate BOS172722. The starting point for our work was a series of pyrido[3,4-*d*]pyrimidine inhibitors that demonstrated excellent potency and kinase selectivity but suffered from rapid turnover in human liver microsomes (HLM). Optimizing HLM stability proved challenging since it was not possible to identify a consistent site of metabolism and lowering lipophilicity proved unsuccessful. Key to overcoming this problem was the finding that introduction of a methyl group at the 6-position of the pyrido[3,4-*d*]pyrimidine core significantly improved HLM stability. Met ID studies suggested that the methyl group suppressed metabolism at the distant aniline portion of the molecule, likely by blocking the preferred pharmacophore through which P450 recognized the compound. This work ultimately led to the discovery of BOS172722 as a Phase 1 clinical candidate.



INTRODUCTION

MPS1 (monopolar spindle 1, also known as TTK) is a dual-specificity kinase that occupies a central role in mitosis. MPS1 is one of the main components of the spindle assembly checkpoint (SAC)^{1–4} and ensures cells do not progress from metaphase to anaphase until the kinetochores are properly attached to the microtubules and under the appropriate tension at the metaphase plate.^{2,3} Cancer cells heavily rely on MPS1 to cope with aneuploidy resulting from aberrant numbers of chromosomes.^{5–8} The kinase has been found to be upregulated in a large number of tumor types^{6,7,9–13} strongly suggesting MPS1 inhibition as a therapeutic approach for the treatment of cancer. As a result, MPS1 inhibitors have been pursued by a number of organizations, and accordingly, at least four compounds have reached Phase 1 clinical trials:

BAY1161909 (1),¹⁴ BAY1217389 (2),¹⁴ CFI-402257 (3),¹⁵ and S 81694 (structure undisclosed). We recently reported advanced inhibitors including CCT251455 (4)¹⁶ and a series of pyrido[3,4-*d*]pyrimidines (34h (5))¹⁷ (Figure 1).

While the single agent efficacy of MPS1 inhibitors has been described to be limited,^{18–21} a number of recent reports have documented that inhibition of MPS1 is particularly effective when used in combination with other drugs, for example, tubulin-targeting agents or CDK4/6 inhibitors.^{22–26} We were particularly intrigued by the use of MPS1 inhibitors in combination with paclitaxel for triple negative breast cancer. Paclitaxel is often used for this aggressive and highly

Received: May 1, 2018

Published: September 10, 2018

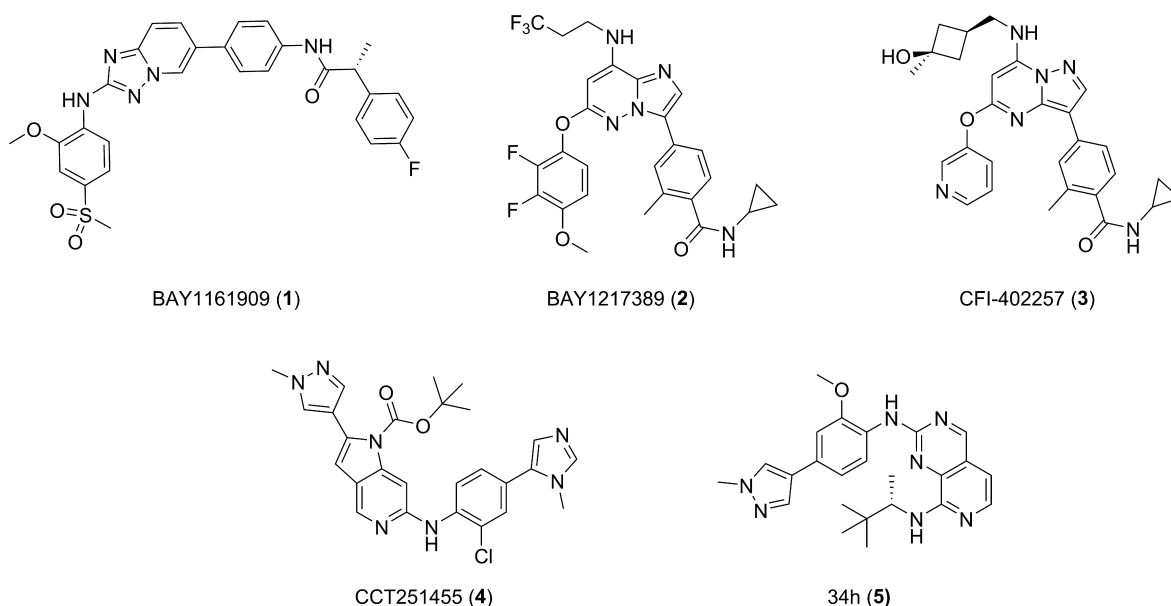


Figure 1. Published MPS1 inhibitors.

proliferative cancer but, on its own, does frequently not lead to durable responses, particularly in the metastatic setting.²⁷ Triple negative breast cancer thus remains a high medical need, and new effective therapeutic regimens are needed.

The work presented here builds upon a series of pyrido[3,4-*d*]pyrimidines that we recently disclosed.¹⁷ Advanced compounds in this series showed excellent potency in biochemical and cellular assays, exemplified by **5** (Figure 2); which was

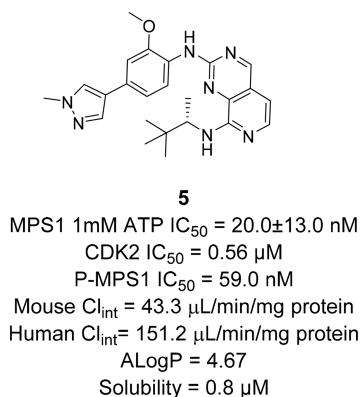


Figure 2. MPS1 inhibitor **5**. “P-MPS1” indicates an electrochemiluminescence mesoscale discovery (MSD)-based cellular assay that measured autophosphorylation of ectopically expressed MPS1 in HCT116 cells. Solubility conditions: HPLC, 1% DMSO, 10 mM PBS, pH 7.4.

effective in inhibiting MPS1 *in vivo*.¹⁷ However, this series in general, and **5** in particular, suffered from key liabilities that prevented further development, specifically high turnover in human microsomes as well as excessive lipophilicity.

Herein, we describe our optimization of the pyrido[3,4-*d*]pyrimidine series¹⁷ culminating in the discovery of a Phase I clinical candidate compound.

CHEMISTRY

Des methyl pyrido[3,4-*d*]pyrimidine compounds were made using the route shown in Scheme 1. Two complementary

approaches could be used to gain access to the des methyl compounds. First, the amine was introduced into **7** by displacement of the chloride, followed by *m*-CPBA oxidation to give sulfone **9**. Displacement of the sulfone with the appropriate formamide under NaH/THF conditions gave rise to the desired des methyl pyrido[3,4-*d*]pyrimidine compounds (Scheme 1). Alternatively, the steps could be reversed, carrying out the *m*-CPBA oxidation as the first step to afford sulfone **18**. Displacement with the appropriate formamide could then be carried out as previously, before introducing the amine at the final step, through reaction of the chloro-intermediate **20** with neopentylamine in NMP at elevated temperatures.

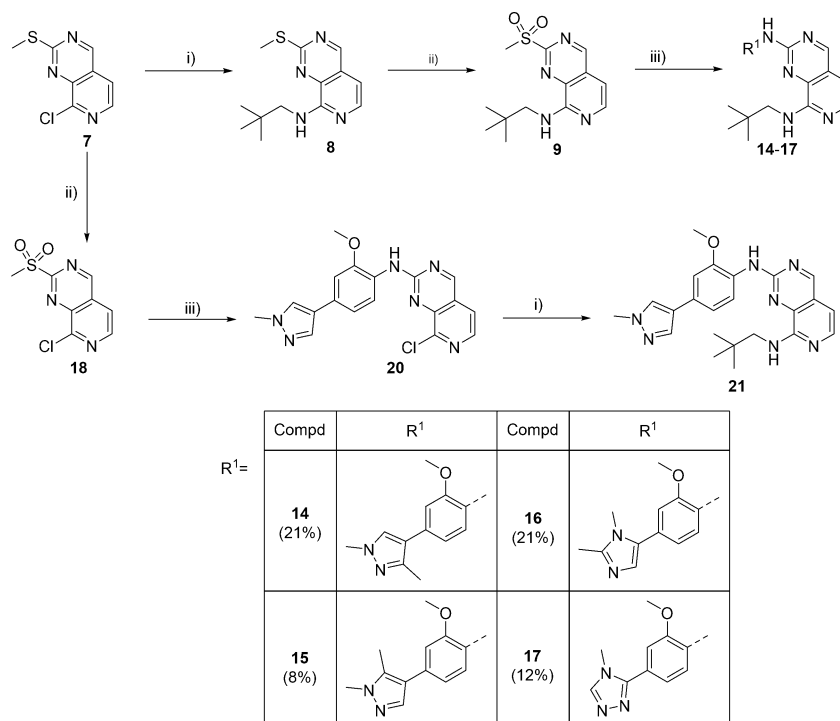
Compounds in the 6-methyl pyrido[3,4-*d*]pyrimidine series were prepared from the key intermediate 8-chloro-2-(methylthio)pyrido[3,4-*d*]pyrimidine **22**, the synthesis of which we have previously reported.²⁸ Treatment of this intermediate with an amine at elevated temperature in NMP gave rise to sulfides **23–25**. Oxidation of these compounds with *m*-CPBA afforded sulfones **26–28**, which were ideally set up to undergo selective displacement. The aniline moiety was introduced using the corresponding formamide with either NaH in THF or cesium carbonate in DMSO, affording the desired 6-methyl pyrido[3,4-*d*]pyrimidines **34–42** (Scheme 2).

Again the order of steps could be reversed with the oxidation with *m*-CPBA being carried out first to give sulfone **43**, which could then undergo the same coupling with the appropriate formamide as previously described using NaH in THF. Displacement of the chloro intermediate **44** was then carried out with amines at elevated temperatures in NMP (Scheme 3).

All amines used were commercially available, and the formamides were synthesized from the corresponding anilines by refluxing in formic acid. The anilines were prepared by standard transformations (see Supporting Information for procedures).

RESULTS AND DISCUSSION

We routinely tested our compounds in a caliper-based MPS1 kinase assay at 1 mM ATP. As described in our preceding publication,¹⁷ this relatively high ATP concentration was

Scheme 1^a

^aReagents and conditions: (i) amine, NMP, 100–130 °C; (ii) *m*-CPBA, CH₂Cl₂, 0 °C–r.t.; (iii) ArNHCHO 10–13 or 19, NaH, THF, 0 °C–r.t.

necessary due to the high potency of advanced compounds (K_i s < 1 nM) that was beyond the dynamic range of the assay at lower ATP concentrations. Furthermore, we progressed compounds of sufficient potency to an MSD-based cellular assay that measured autophosphorylation of ectopically expressed MPS1 in HCT116 cells.¹⁶ In addition, we routinely determined selectivity against CDK2, a cell cycle kinase with a high homology to MPS1 in terms of the ATP binding domain. Since the CDK2 assay was run at much lower ATP concentrations, we converted the IC₅₀ values from the MPS1 assay (at 1 mM ATP) and those from the CDK2 assay (at 10 μM ATP) into K_i values and used these calculated K_i s to assess the selectivity ratio.

Our key goal for the optimization of the pyrido[3,4-*d*]pyrimidines series was to significantly improve the low human liver microsomal stability observed for compound 5 and other compounds in this series. Extensive attempts to identify major metabolites showed multiple oxidations and dealkylation products but failed to identify a consistent site of metabolism. Furthermore, we had not observed a correlation between stability in human microsomes and lipophilicity indicating that lowering LogP was not a promising approach. We thus suspected that rapid turnover was driven by recognition of a specific pharmacophore within our series and decided to systematically derivatize the molecule to discover modifications that would block this recognition and increase the metabolic stability.

We started by altering the five-membered ring heterocycle of 5 maintaining a neopentyl substituent in the 8-position of the pyrido[3,4-*d*]pyrimidine core. These compounds are summarized in Table 1. Methylated and dimethylated pyrazole containing compounds (21, 14, and 15) showed only relatively modest activity in the high ATP assay, as well as in the cellular assay. The imidazole substituted compound (16) demon-

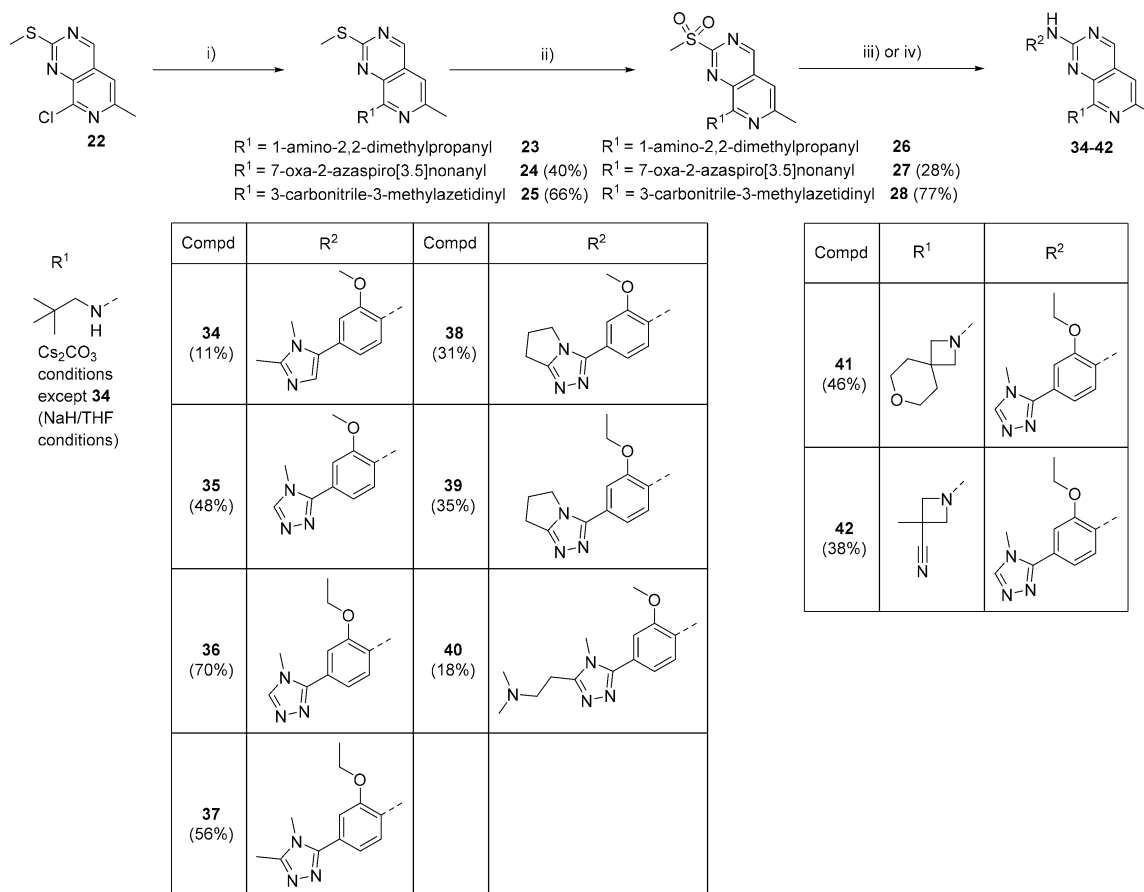
strated excellent levels of biochemical activity, as well as showing promising levels of selectivity over CDK2 and cellular activity. Finally, triazole containing 17, while exhibiting nanomolar potency for CDK2, stood out in terms of its single digit nanomolar potency in the cellular assay and represents one of the most potent MPS1 inhibitors known to us. In fact, the potency of this compound was beyond the lower range of our biochemical assay even at 1 mM ATP. The reason why replacing the pyrazole moiety in 21 with imidazole (15) and particularly triazole (16) significantly boosted biochemical activity remained unclear, and crystal structures (*vide infra*) did not provide any additional insights.

We tested the human liver microsome (HLM) stability of compounds 16 and 17, but both still underwent extensive metabolism showing Cl_{int} values of 79 and 92 μL/min/mg protein, respectively. Nevertheless, the comparably low molecular weight (418) and lipophilicity (3.6) made 17 an excellent starting point for further investigation, and we decided to improve CDK2 selectivity and HLM stability.

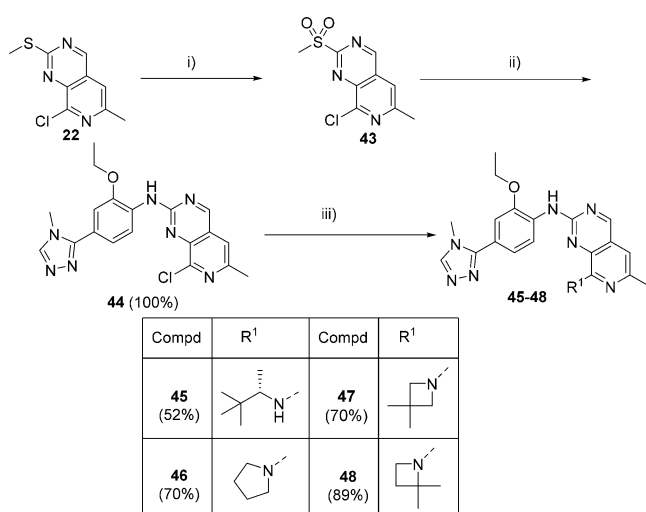
In order to develop hypotheses on how to reduce CDK2 activity, we superimposed X-ray structures of our compounds¹⁷ with published CDK2 structures (Figure 3).^{29,30}

Fourteen residues are different within the ATP binding pockets of MPS1 and CDK2, including the gatekeeper residue, which is Met602 in MPS1 and a bulkier phenylalanine (Phe80) in CDK2 (Figure 3). We hypothesized that introducing a methyl group at the 6-position of the pyrido[3,4-*d*]pyrimidine core would be less tolerated in CDK2 than in MPS1, due to a clash with the CDK2 Phe80 gatekeeper residue.

We thus set out to prepare a series of methyl substituted compounds. The significant investigations required to access pyrido[3,4-*d*]pyrimidines with substitution in this position were disclosed by us recently.²⁸

Scheme 2^a

^aReagents and conditions: (i) amine, NMP, 100–130 °C; (ii) *m*-CPBA, CH₂Cl₂, 0 °C–r.t.; (iii) ArNHCHO **12**, **13**, or **29–33**, NaH, THF, 0 °C–r.t.; (iv) ArNHCHO, Cs₂CO₃, DMSO, 120 °C.

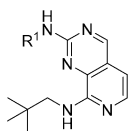
Scheme 3^a

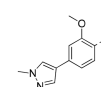
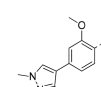
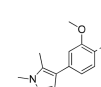
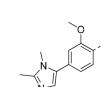
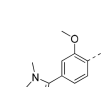
^aReagents and conditions: (i) *m*-CPBA, CH₂Cl₂, 0 °C–r.t.; (ii) ArNHCHO **29**, NaH, THF, 0 °C–r.t.; (iii) amine, NMP, 100–130 °C.

Table 2 shows the biochemical and cellular results for two initial proof-of-concept compounds made as matched pairs to the corresponding unsubstituted compounds (**16** and **17**). Both compounds show potent biochemical inhibition of MPS1

and lower but still acceptable levels of inhibition in cells. As hypothesized, both 6-methylated compounds (**34** and **35**) demonstrated a significant improvement in selectivity for MPS1 over CDK2 (K_i ratio is between 500 and 7600). Even more importantly and somewhat unexpectedly, we observed a large improvement in HLM metabolism for the 6-methylated compounds. Compounds **34** and **35** represented by far the most stable compounds we had observed and thus a breakthrough in terms of optimizing the up to this point persisting HLM liability. We thus decided to focus on the methylated amino-pyrido[3,4-*d*]pyrimidine core.

To understand why these compounds showed greatly improved stability, we identified the metabolites for the matched pair **17** and **35**. Interestingly, these experiments showed that the introduction of the methyl group completely changed the nature of the main metabolites in HLM (Figure 4). Incubation of compound **17** with HLM primarily led to metabolites in which the triazole and aniline moieties were oxidized (Figure 4). In sharp contrast, treatment of **35** with HLM led to oxidation on the neopentyl chain followed by loss of the entire chain (Figure 4). Importantly, the metabolic hotspots are not only different for these compounds but, in both cases, also distant from the position of the newly introduced methyl group of **35**. This observation thus suggests that the reduction of HLM metabolism is not due to blocking of a metabolically labile position (a commonly applied strategy, particularly using fluorine atoms) but instead to blocking of the

Table 1. Biochemical and Cellular Data for Aniline Modifications on Neopentyl-Substituted Core^a


Compd	R ¹	Biochemical activity				P-MPS1 IC ₅₀	AlogP
		MPS1		CDK2			
		IC ₅₀	K _i	IC ₅₀	K _i		
21		44	0.44	450	230	140	4.27
14		2,500	24	2,800	1,400	230	4.56
15		79	0.78	3,000	1,500	95	4.42
16		8.5	0.084	86	43	44	4.27
17		≤ 6.8	≤ 0.07	16	8.0	3.5	3.60

^aResults are in nM unless otherwise stated and are mean for $n \geq 3$, or mean values of two independent determinations or samples run $n = 1$. For SD (for $n \geq 3$) and individual determinations ($n = 2$), see Table S1. "P-MPS1" indicates an electrochemiluminescence mesoscale discovery (MSD)-based cellular assay that measured autophosphorylation of ectopically expressed MPS1 in HCT116 cells. K_i s were calculated from the IC₅₀s using the Cheng–Prusoff equation.

pharmacophore through which 17 is recognized and bound. This hypothesis is consistent with the nature of P450 enzymes where substrate recognition and catalytic sites are spatially separated.

Compound 35 thus represented a significant step forward, and we explored whether HLM stability, CDK2 selectivity, cellular potency, and solubility could be further optimized. Table 3 summarizes modifications of the methoxy group and the triazole ring substituents. Based on existing SAR, we hypothesized that introducing an ethoxy group in place of the methoxy group of 35 improves selectivity further. The corresponding ethoxy compound (36) showed similar levels of biochemical potency (IC₅₀ 11 vs 13 nM), albeit with a slight drop in cellular potency (P-MPS1 IC₅₀ 63 vs 30 nM). As hypothesized, this transformation resulted in an improved selectivity window over CDK2 (K_i ratio 500 (35) vs 46 (36)) and significantly improved stability in HLM.

Introduction of a methyl group onto the triazole ring (37) resulted in very similar levels of potency to 35 both in the biochemical and cellular assays (Table 3), albeit with an increase in lipophilicity (AlogP = 4.49 vs 3.88). The bicyclic triazole derivatives 38 and 39 were also potent biochemical inhibitors but showed significantly weaker inhibition in cells.

Interestingly, this matched pair (38 and 39) also demonstrated a similar increase in selectivity between methoxy and ethoxy derivatives. Finally, adding a basic dimethylamino group to improve solubility (40) resulted in loss of cellular potency (P-MPS1 IC₅₀ 230 nM) possibly due to a decrease in cellular permeability of the more polar dimethylamine tail group, though the solubility (77.6 μ M [HPLC method, 1% DMSO, 10 mM PBS, pH 7.4]) of this compound was greatly improved in comparison to 35.

From this investigation, 36 emerged as an attractive compound, and we tested if the overall properties could be further optimized by modification of the neopentyl amine.

Table 4 shows a representative set of amine substitutions at the 8-position of the pyrido[3,4-*d*]pyrimidine core. Compound 45 bears the same branched primary amine used in our previously reported MPS1 inhibitor 5.¹⁷ Compound 45 demonstrated good activity against MPS1 in the biochemical and cellular assays (Table 4) but exhibits poor solubility (2.2 μ M), a possible consequence of the increased AlogP (4.61). The introduction of secondary amines including pyrrolidine (46) and substituted azetidines (47, 48, and 42) exhibited varied activity against MPS1. Pyrrolidine containing 46 displayed a significant decrease in the biochemical and cellular

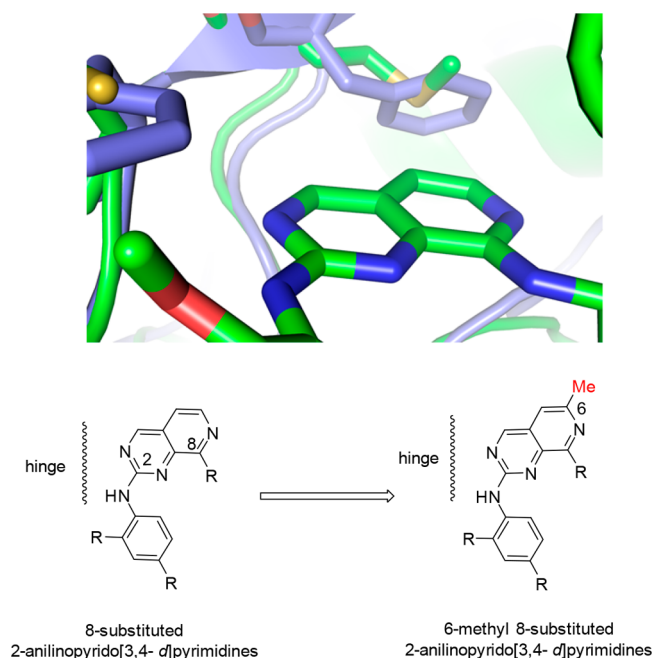


Figure 3. Top: Superimposed crystal structure of MPS1 (green) bound to a pyrido[3,4-*d*]pyrimidine core (carbon atoms colored green), extracted from PDB code 5EH0, onto the structure of CDK2 (blue), extracted from PDB code 1H08 (ligand hidden for clarity), showing the different gatekeeper residues present in MPS1 and CDK2. Bottom: 6-position methyl group on pyrido[3,4-*d*]pyrimidine core.

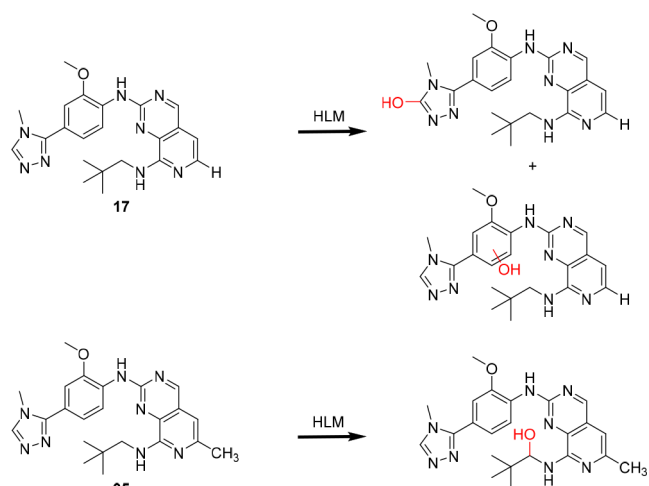


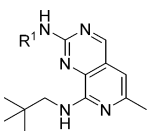
Figure 4. Results of a Met ID study showing oxidation products for the match pair of compounds 17 and 35 after treatment with HLM.

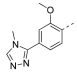
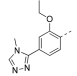
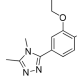
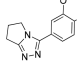
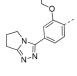
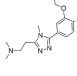
potency observed. Compound 47 exhibited excellent activity (P-MPS1 IC₅₀ 37 nM) and good levels of selectivity over CDK2 coupled with an increased solubility of 31.5 μM, possibly due to the decreased ALogP of 3.85. However, movement of the gem dimethyl group one carbon round the ring into the α-position (48) resulted in loss of all MPS1 activity (P-MPS1 IC₅₀ 3.8 μM). Cyano-substituted azetidine compound (42) also showed acceptable levels of potency (P-MPS1 IC₅₀ 110 nM) and selectivity over CDK2 (CDK2 IC₅₀

Table 2. Biochemical and Cellular Data for Two Matched Pairs of Compounds Containing H or Me at the 6-Position of the Pyrido[3,4-*d*]pyrimidine Core^a

Compd	Structure	Biochemical activity				P-MPS1 IC ₅₀	AlogP	Cl _{int} (μL/min/mg protein)	
		MPS1		CDK2				mouse	human
		IC ₅₀	K _i	IC ₅₀	K _i				
16		8.5	0.084	86	43	44	4.27	92.5	79.4
34		9.5	0.094	1,400	720	170	4.55	34.5	28.2
17		6.8	0.067	16	8.0	3.5	3.60	81.5	92.1
35		13	0.13	130	65	30	3.88	41.1	23.8

^aResults are in nM unless otherwise stated and are mean for $n \geq 3$, or mean values of two independent determinations or samples run $n = 1$. For SD (for $n \geq 3$) and individual determinations ($n = 2$), see Table S2. "P-MPS1" indicates an electrochemiluminescence mesoscale discovery (MSD)-based cellular assay that measured autophosphorylation of ectopically expressed MPS1 in HCT116 cells. K_i s were calculated from the IC₅₀s using the Cheng–Prusoff equation.

Table 3. Biochemical and Cellular Data for Triazole Modifications Based on 35^a


Compd	R ¹	Biochemical activity				P-MPS1 IC ₅₀	AlogP	Cl _{int} (μL/min/mg protein)		Solubility μM
		MPS1		CDK2				mouse	human	
		IC ₅₀	K _i	IC ₅₀	K _i					
35		13	0.13	130	65	30	3.88	41.1	23.8	8.6
36		11	0.11	1,020	510	63	4.23	26.3	8.0	6.6
37		12	0.12	940	470	33	4.49	32.9	20.4	1.8
38		19	0.19	250	130	240	4.40	28.8	28.8	1.7
39		38	0.38	>10,000	>5,000	250	4.75	36.4	18.6	nd
40		12	0.12	360	180	230	4.75	27.7	23.0	77.6

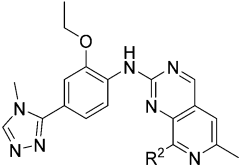
^aResults are in nM unless otherwise stated and are mean for $n \geq 3$, or mean values of two independent determinations or samples run $n = 1$. For SD (for $n \geq 3$) and individual determinations ($n = 2$), see Table S3. "P-MPS1" indicates an electrochemiluminescence mesoscale discovery (MSD)-based cellular assay that measured autophosphorylation of ectopically expressed MPS1 in HCT116 cells.

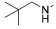
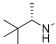
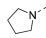
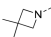
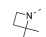
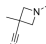
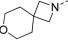
2.70 μM), combined with a much lower AlogP of 3.25. However, this reduced ALogP did not translate into increased solubility, with 42 only showing a solubility of 6.8 μM. Introduction of a polar spirocyclic amine (41) resulted in a dramatic drop in lipophilicity (AlogP = 3.08), which, as expected, translated into an increase in solubility (56.2 μM).

To understand the observed MPS1 SAR (Table 4), we solved the crystal structure of compound 36 bound to MPS1 (Figure 5A). As expected, the binding mode of 36 was nearly identical to that of the previously described pyrido[3,4-*d*]pyrimidine inhibitors.¹⁷ The pyrido[3,4-*d*]pyrimidine scaffold of 36 binds to the hinge region, the 6-methyl group important for CDK2 selectivity and for the reduction in HLM metabolism, is located close to the side chain of the gatekeeper residue Met602, and the ethoxy moiety also important for selectivity binds in the selectivity pocket above the hinge. Somewhat surprisingly, the triazole moiety was not engaged in a hydrogen bond, and thus the X-ray structure did not explain why replacing the pyrazole of 21 with triazole (17, Table 1) led to a significant increase in activity (*vide supra*). Together with previously reported structures of CCT251455 (4) and (5), the X-ray structure of 36 allowed us to rationalize the SAR

summarized in Table 4. As previously described for compound 5, the neopentyl chain binds to a hydrophobic pocket that is created by a reordering of the MPS1 activation loop into an inactive conformation (Figure 5B).^{16,17} The shape of the neopentyl chain represents an excellent match to this pocket resulting in several hydrophobic contacts explaining why this moiety is critical for activity. The two azetidines derivatives 47 and 48 exemplify the importance of the correct shape of the amine substituent for potent inhibition. The 3,3-dimethylazetidines substituent of derivative 47 can be regarded as a constrained mimetic of the neopentyl chain that can likely engage in similar hydrophobic contacts, and 47 maintains potent inhibition. The 2,2-dimethylazetidines moiety of 48, however, differs significantly in its overall shape from the neopentyl chain leading to less favorable interactions and a 40-fold higher IC₅₀.

To investigate which of the potent and selective compounds in Table 4 can be progressed further, we tested the stability in liver microsomes. Gratifyingly, all compounds tested showed satisfactory stability (Cl_{int} < 45 μL/min/mg protein in mouse and Cl_{int} < 26 μL/min/mg protein in human) (Table 4). This represented a vast improvement over the human intrinsic

Table 4. Biochemical and Cellular Data for Amine Modifications Based on 36^a


Compd	R ²	Biochemical activity				P-MPS1 IC ₅₀	AlogP	Cl _{int} (μL/min/mg protein)		Solubility μM
		MPS1 (1 mM ATP)		CDK2				mouse	human	
		IC ₅₀	K _i	IC ₅₀	K _i					
36		11	0.11	1,020	510	63.0	4.23	26.3	8.0	6.6
45		4.7	0.047	150	77	23.0	4.61	25.3	15.2	2.2
46		83	0.82	1,100	550	370	3.58	nd	nd	nd
47		8.9	0.088	1,600	810	37	3.85	44.3	25.2	31.5
48		400	4.0	26,000	13,000	3,800	3.58	nd	nd	nd
42		20	0.20	2,700	1,400	110	3.25	24.7	5.6	6.8
41		11	0.11	2,500	1,300	37	3.08	32.9	9.4	56.2

^aResults are in nM unless otherwise stated and are mean for $n \geq 3$, or mean values of two independent determinations or samples run $n = 1$. For SD (for $n \geq 3$) and individual determinations ($n = 2$), see Table S4. “P-MPS1” indicates an electrochemiluminescence mesoscale discovery (MSD)-based cellular assay that measured autophosphorylation of ectopically expressed MPS1 in HCT116 cells.

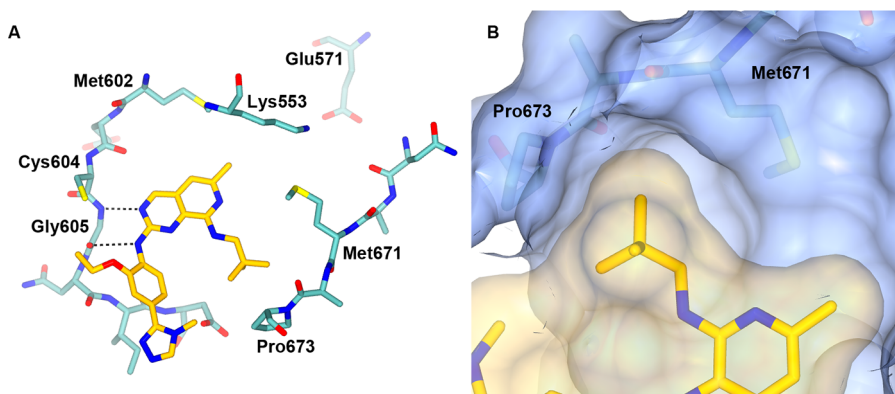
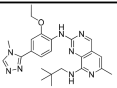
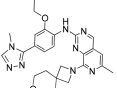
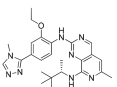
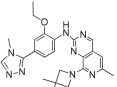


Figure 5. (A) Crystal structure of 36 bound to MPS1 (pdb code 6H3K). Compound 36 is shown with carbon atoms in yellow. Selected amino acids are shown in sea green and are labeled. Key hydrogen bonds are indicated as black dotted lines. (B) Close up of the neopentyl binding pocket. The neopentyl substituent is enveloped by residues Met671 and Pro673 from the activation loop. Protein surface is displayed as a transparent blue surface. The compound surface is shown in transparent yellow.

Table 5. Mouse and Rat Blood Pharmacokinetics of 36, 41, 45, and 47 at 5 mg/kg iv and po, unless Otherwise Stated^{a,b,c}

Compd	Structure	species	t _{1/2} (h)	Cl (mL/min/kg)	C _{max} _{po} (nmol/L)	AUC _{po} (h*nmol/L) ^d	PPB (%)	V _{ss} (L/kg)	F (%)
36		mouse	2.68	10.9	2757	11000	99.85	2.46	81
		rat ^a	4.66	10.1	813	11325	nd	3.52	63
41		mouse	0.66	22.6	3083	4779	98.09	1.21	63
		rat	1.5	7.59	1181	5156 ^e	nd	0.89	22
45		mouse	3.47	8.40	2923	13764	99.91	2.19	86
		rat ^b	4.52	6.00	1893	273000	nd	1.88	92
47		mouse	1.58	16.3	2348	8110	99.28	2.09	75
		rat	3.03	7.35	1417	18335	nd	1.88	72

^a2.5 mg/kg (iv). ^b1 mg/kg (iv). ^cCompounds were administered iv and po (Mouse, 0.1 mL/10 g in 10% DMSO, 5% Tween 20 in saline; Rat, 0.05 mL/10 g in 10% DMSO, 5% Tween 20 in saline). ^dAUC_{last} 6 h for mouse, 24 h for rat, unless otherwise stated. ^eAUC_{last} 6 h.

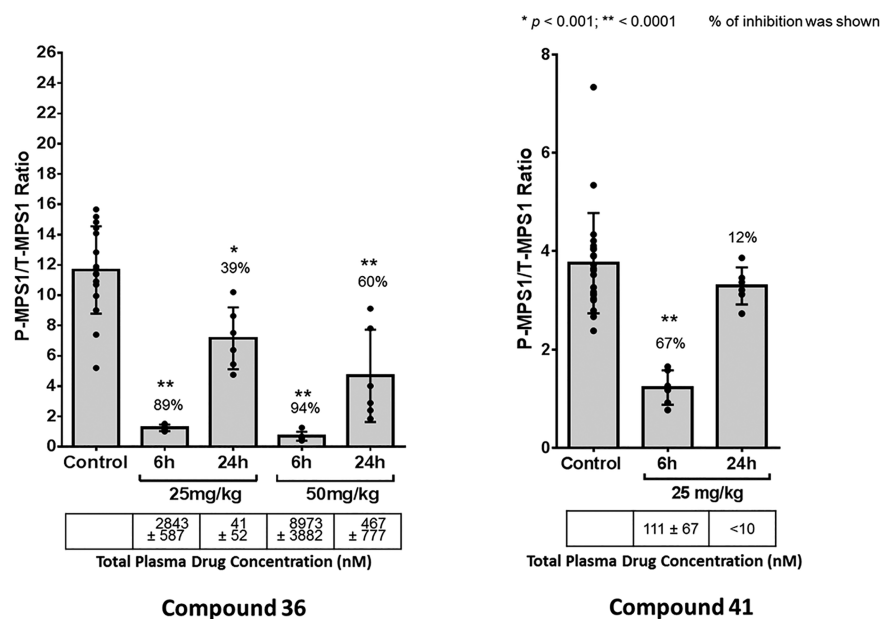


Figure 6. Bar charts show the ratio of phosphorylated-MPS1/total-MPS1 levels (gray) in the Dox-DLD1 model after treatment with 36 (left) and 41 (right) at specified doses and time points. The plasma levels at the respective time points are given in the table below the bar chart.

clearance values seen for compound 5 (Cl_{int} 151.2 μL/min/mg protein), the starting point of our investigation.

With a number of active, selective, and soluble compounds in hand, we decided to investigate the mouse and rat pharmacokinetics (PK) of a selection of compounds (36, 45, 47, and 41) at 5 mg/kg administered both intravenous (iv) and orally (po) (Table 5).³¹ The resulting data showed moderate clearance for all compounds in both mouse (8.4–22.6 mL/min/kg) and rat (6.00–10.1 mL/min/kg). All compounds with the exception of 41 showed high oral bioavailability in both species (63–92%) with moderate volumes of distribution (Table 5). The plasma protein binding for all four of these compounds was high (>98%), the lowest unsurprisingly shown by that presenting the lowest AlogP

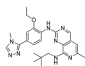
(41). This corresponded to a higher blood clearance and shorter half-life (0.66 h) for 41 compared to 36 (2.68 h).

We thus decided to progress both 36 and 41 to a single dose pharmacokinetic/pharmacodynamic (PK/PD) experiment in DLD1 xenografts to investigate if the *in vitro* and PK profiles translated into sustained inhibition of MPS1 *in vivo* (Figure 6). We recently disclosed³² a xenograft model to assess modulation of MPS1 activity *in vivo*. Briefly, this model (Dox-DLD1) measures the level of MPS1 autophosphorylation in DLD1 cancer cells and, importantly, overcomes the issue of low MPS1 levels through doxycycline inducible expression of the kinase. We tested both compounds at 25 mg/kg and in addition compound 36 at 50 mg/kg. The data are summarized in Figure 6. At 25 mg/kg, both compounds led to a pronounced reduction of MPS1 autophosphorylation after 6

h. Consistent with its longer half-life, only **36** showed significant inhibition at 24 h. As expected, the 50 mg/kg dose of **36** resulted in an increased suppression of MPS1 autophosphorylation at 6 and 24 h. The comparison of the plasma levels determined in the PK/PD study (Figure 6) after blood to plasma correction with the compound levels determined in the PK study described above and performed at lower doses (Table 5) was consistent with linear PK.

The robust modulation of the PD biomarkers observed for **36** prompted us to focus on this compound since a long duration of action is desirable for cell cycle targets. At 1 mg/kg iv and 5 mg/kg po, **36** showed complete bioavailability (100%), low clearance (1.2 mL/min/kg), a moderate volume of distribution (1.1 L/kg), and a 12 h half-life (Table 6) in a dog PK study.

Table 6. Dog Blood Pharmacokinetics not Dogblood 36 at 1 mg/kg iv and 5 mg/kg po^a

Compd	Structure	species	t _{1/2} (h)	Cl (mL/min/kg)	C _{max} po (nmol/L)	AUC _{po} (h ² nmol/L) ^b	V _d (L/kg)	F (%)
36		dog	12	1.2	7770	147035	1.1	100

^aThe compound was administered as the dichloride salt in saline containing 10% DMSO. ^bAUC_{last} 48 h.

We were intrigued by the high bioavailability of **36**, particularly given its poor solubility. Interestingly, pK_a values for **36** were determined as 6.22 and 2.63. This suggests that, while the compound primarily exists as the free base at physiological pH, it is protonated in the acidic environment of the stomach, likely accelerating the dissolution and enabling high bioavailability despite modest solubility at physiological pH. This is an attractive feature of the pyrido [3,4-*d*]pyrimidine scaffold since it avoids the well-recognized risk associated with drugs carrying a positive charge at physiological pH, namely, hERG inhibition, efflux, and detrimental effects on passive permeation while still allowing high bioavailability and salt formation. To shed light on the question of which atom represents the weakly basic center, we performed a calculation using MoKa.³³ This calculation predicted that the nitrogen atom of the pyridine ring is by far the most basic atom.

To complete the *in vitro* profiling, **36** was tested in a wide panel of more than 400 kinases (Supporting Information, Tables S5–S8). As we had seen with our previous MPS1 inhibitor **5**,¹⁷ only a small number of other kinases were inhibited by **36**, in particular JNK1, JNK2, JNK3, and LRRK2 at >80% at 1 μM. Follow up IC₅₀ values were obtained (JNK1 IC₅₀ = 92 nM, JNK2 IC₅₀ = 76 nM, JNK3 IC₅₀ = 242 nM, and LRRK2 IC₅₀ = 48 nM) showing that **36** is selective for MPS1 over these other kinases. Furthermore, **36** also showed a clean CYP and hERG profile (Supporting Information, Tables S9 and S10).

Following extensive *in vivo* testing, particularly in combination with paclitaxel, the results of which will be published in due course (manuscript in preparation), we nominated **36** as our candidate. The synthesis of **36** has been scaled up into the kilogram range, and the drug is currently undergoing Phase 1 clinical trials.

CONCLUSIONS

We describe herein the discovery of our MPS1 inhibitor **36** (BOS172722). The starting point for the work described here was a series of previously reported pyrido[3,4-*d*]pyrimidine inhibitors. These earlier compounds already showed promising *in vitro* potency and selectivity but suffered from a number of liabilities, particularly high lipophilicity and rapid metabolism in HLM. Optimizing HLM metabolism proved challenging since commonly used approaches, such as identification of metabolites and lowering lipophilicity, did not help. Key to overcoming this problem was the serendipitous finding that introduction of a methyl group at the 6-position of the pyrido[3,4-*d*]pyrimidine core significantly improved HLM stability. Met ID studies suggested that the methyl group suppressed metabolism at the distant aniline portion of the molecule, likely by blocking the preferred pharmacophore through which P450 recognized the compound. Compound **17** is thus an interesting example where metabolism is not primarily driven by hydrophobicity or the presence of a particular metabolic hotspot but by recognition of a specific pharmacophore distant from the site of metabolism. These results underscore the importance of systematic chemical modification to solve high metabolic turnover.

Further optimization led to a set of compounds with promising *in vitro* profile, and we progressed a number of selected compounds to PK and subsequently PK/PD experiments. Compound **36** emerged as our candidate showing excellent PK in mouse, rat, and dog. Data showing robust efficacy of **36** in combination with paclitaxel in *in vivo* models will be published shortly.

Interestingly, **36** showed very good bioavailability in all three species despite very modest solubility at physiological pH. We attribute this observation to the weakly basic character of **36** (pK_a = 6.22) and other compounds in this series, which is likely accelerating their dissolution in the acidic environment of the stomach.

The synthesis of **36** has been scaled to the kilogram range, and the compound is currently in Phase 1 clinical trials.

EXPERIMENTAL SECTION

General Chemistry Information. Starting materials, reagents, and solvents for reactions were reagent grade and used as purchased. Chromatography solvents were HPLC grade and were used without further purification. Thin layer chromatography (TLC) analysis was performed using silica gel 60 F-254 thin layer plates. Flash column chromatography was carried out using columns prepacked with 40–63 μm silica. Microwave-assisted reactions were carried out using a Biotage Initiator microwave system. LCMS and HRMS analyses were performed on a HPLC system with diode array detector operating at 254 nm, fitted with a reverse-phase 50 × 4.6 mm column at a temperature of 22 °C, connected to a time of flight (ToF) mass spectrometer (ESI). The following solvent system, at a flow rate of 2 mL/min, was used: solvent A, methanol; solvent B, 0.1% formic acid in water. Gradient elution was as follows: 1:9 (A:B) to 9:1 (A:B) over 2.5 min, 9:1 (A:B) for 1 min then reversion back to 1:9 (A:B) over 0.3 min, 1:9 (A:B) for 0.2 min. ¹H NMR spectra were recorded on a Bruker Avance 500 MHz spectrometer using an internal deuterium lock. NMR data is given as follows: chemical shift (δ) in ppm, multiplicity, coupling constants (*J*) given in Hz, and integration. The purity of final compounds was determined by HPLC as described above and is ≥95% unless specified otherwise.

Compounds 8-chloro-2-(methylthio)pyrido[3,4-*d*]pyrimidine²⁸ **7**, 2-(methylthio)-*N*-neopentylpyrido[3,4-*d*]pyrimidin-8-amine²⁸ **8**, 2-(methylsulfonyl)-*N*-neopentylpyrido[3,4-*d*]pyrimidin-8-amine²⁸ **9**, 8-chloro-2-(methylsulfonyl)pyrido[3,4-*d*]pyrimidine²⁸ **18**, *N*-(2-me-

thoxy-4-(1-methyl-1*H*-pyrazol-4-yl)phenyl)formamide²⁸ **19**, 8-chloro-*N*-(2-methoxy-4-(1-methyl-1*H*-pyrazol-4-yl)phenyl)pyrido[3,4-*d*]pyrimidin-2-amine²⁸ **20**, *N*²-(2-methoxy-4-(1-methyl-1*H*-pyrazol-4-yl)phenyl)-*N*⁸-neopentylpyrido[3,4-*d*]pyrimidine-2,8-diamine^{17,28} **21**, 8-chloro-6-methyl-2-(methylthio)pyrido[3,4-*d*]pyrimidine²⁸ **22**, 6-methyl-2-(methylthio)-*N*-neopentylpyrido[3,4-*d*]pyrimidin-8-amine²⁸ **23**, and 6-methyl-2-(methylsulfonyl)-*N*-neopentylpyrido[3,4-*d*]pyrimidin-8-amine²⁸ **26** were synthesized by previously reported methods.

Preparation of Compounds in Scheme 1. General Procedure for NaH Mediated Displacement on 9 (Compounds 14–17). To a cooled (0 °C) solution of appropriate formamide (1 equiv) in THF (3 mL) was added sodium hydride (60% dispersion in oil, 1.6 equiv). The reaction mixture was stirred at r.t. for 10 min. The reaction mixture was cooled to 0 °C, and appropriate sulfone (1.2 equiv) was added. The reaction mixture was stirred for 18 h, while slowly warming to r.t. aq NaOH (1 M, 1 mL) and MeOH (1 mL) were added, and the reaction mixture was stirred at r.t. for 1 h. The reaction mixture was concentrated *in vacuo*, and the residue was diluted with EtOAc and water. The aqueous layer was re-extracted with EtOAc and CH₂Cl₂. The combined organic layers were washed with water and brine, dried (MgSO₄), and concentrated *in vacuo*. The residue was purified by flash column chromatography (0–10% MeOH in EtOAc or CH₂Cl₂) and, if necessary, followed by SCX-2 cartridge (MeOH, 1 M NH₃ in MeOH) to afford the title compounds.

*N*²-(4-(1,3-Dimethyl-1*H*-pyrazol-4-yl)-2-methoxyphenyl)-*N*⁸-neopentylpyrido[3,4-*d*]pyrimidine-2,8-diamine **14**. Using *N*-(4-(1,3-dimethyl-1*H*-pyrazol-4-yl)-2-methoxyphenyl)formamide **10** and 2-(methylsulfonyl)-*N*-neopentylpyrido[3,4-*d*]pyrimidin-8-amine **9**.²⁸ Yield = 21%. HRMS (ESI) *m/z* calcd for C₂₄H₃₀N₇O (M + H) 432.2506, found 432.2502; ¹H NMR (500 MHz, CD₃OD) δ 9.07 (s, 1H), 8.42 (d, *J* = 8.0 Hz, 1H), 7.73 (s, 1H), 7.71 (d, *J* = 6.0 Hz, 1H), 7.10 (d, *J* = 1.5 Hz, 1H), 7.03 (dd, *J* = 8.0, 1.5 Hz, 1H), 6.85 (d, *J* = 6.0 Hz, 1H), 4.00 (s, 3H), 3.88 (s, 3H), 3.40 (s, 2H), 2.40 (s, 3H), 1.09 (s, 9H).

*N*²-(4-(1,5-Dimethyl-1*H*-pyrazol-4-yl)-2-methoxyphenyl)-*N*⁸-neopentylpyrido[3,4-*d*]pyrimidine-2,8-diamine **15**. Using *N*-(4-(1,5-dimethyl-1*H*-pyrazol-4-yl)-2-methoxyphenyl)formamide **11** and 2-(methylsulfonyl)-*N*-neopentylpyrido[3,4-*d*]pyrimidin-8-amine **9**.²⁸ Yield = 8%. HRMS (ESI) *m/z* calcd for C₂₄H₃₀N₇O (M + H) 432.2506, found 432.2504; ¹H NMR (500 MHz, CDCl₃) δ 9.02 (s, 1H), 8.51 (br s, 1H), 8.05 (m, 1H), 7.84 (m, 1H), 7.58 (s, 1H), 6.99 (dd, *J* = 8.2, 1.8 Hz, 1H), 6.96 (d, *J* = 1.8 Hz, 1H), 6.80 (br s, 1H), 3.99 (s, 3H), 3.88 (s, 3H), 3.64 (br s, 2H), 2.42 (s, 3H), 1.14 (s, 9H).

*N*²-(4-(1,2-Dimethyl-1*H*-imidazol-5-yl)-2-methoxyphenyl)-*N*⁸-neopentylpyrido[3,4-*d*]pyrimidine-2,8-diamine **16**. Using *N*-(4-(1,2-dimethyl-1*H*-imidazol-5-yl)-2-methoxyphenyl)formamide **12** and 2-(methylsulfonyl)-*N*-neopentylpyrido[3,4-*d*]pyrimidin-8-amine **9**.²⁸ Yield = 21%. HRMS (ESI) *m/z* calcd for C₂₄H₃₀N₇O (M + H) 432.2506, found 432.2504; ¹H NMR (500 MHz, CDCl₃) δ 9.04 (s, 1H), 8.76 (d, *J* = 8.0 Hz, 1H), 8.12 (s, 1H), 7.94 (d, *J* = 6.0 Hz, 1H), 7.21 (s, 1H), 6.99 (dd, *J* = 8.0, 2.0 Hz, 1H), 6.91 (d, *J* = 2.0 Hz, 1H), 6.79 (d, *J* = 6.0 Hz, 1H), 6.58 (br s, 1H), 4.02 (s, 3H), 3.67 (s, 3H), 3.50 (d, *J* = 6.0 Hz, 2H), 2.82 (s, 3H), 1.12 (s, 9H).

*N*²-(2-Methoxy-4-(4-methyl-4*H*-1,2,4-triazol-3-yl)phenyl)-*N*⁸-neopentylpyrido[3,4-*d*]pyrimidine-2,8-diamine **17**. Using *N*-(2-methoxy-4-(4-methyl-4*H*-1,2,4-triazol-3-yl)phenyl)formamide **13** and 2-(methylsulfonyl)-*N*-neopentylpyrido[3,4-*d*]pyrimidin-8-amine **9**.²⁸ Yield = 12%. HRMS (ESI) *m/z* calcd for C₂₂H₂₇N₈O (M + H) 419.2302, found 419.2288; ¹H NMR (500 MHz, CD₃OD) δ 9.15 (s, 1H), 8.74 (d, *J* = 8.5 Hz, 1H), 8.57 (s, 1H), 7.77 (d, *J* = 6.0 Hz, 1H), 7.43 (d, *J* = 1.5 Hz, 1H), 7.35 (dd, *J* = 8.5, 1.5 Hz, 1H), 6.90 (d, *J* = 6.0 Hz, 1H), 4.07 (s, 3H), 3.87 (s, 3H), 3.44 (s, 2H), 1.10 (s, 9H).

Preparation of Compounds in Scheme 2. General Procedure for Amine Displacement on 22. To a solution of 8-chloro-6-methyl-2-(methylthio)pyrido[3,4-*d*]pyrimidine **22** (1 equiv) in NMP (20 mL) was added appropriate amine (2 equiv) and triethylamine (5 equiv). The reaction mixture was heated to 100 °C for 36 h. The reaction mixture was diluted with EtOAc and water, dried (MgSO₄), and concentrated *in vacuo*. The residue was purified by flash column

chromatography (0–50% EtOAc in cyclohexane) to afford the title compounds.

2-(6-Methyl-2-(methylthio)pyrido[3,4-*d*]pyrimidin-8-yl)-7-oxa-2-azaspiro[3.5]nonane **24**. Using 7-oxa-2-azaspiro[3.5]nonane. Yield = 40%. HRMS (ESI) *m/z* calcd for C₁₆H₂₁N₄O₂ (M + H) 317.1431, found 317.1422; ¹H NMR (500 MHz, CD₃OD) δ 9.00 (s, 1H), 6.76 (app s, 1H), 4.33 (br s, 4H), 3.71 (app t, *J* = 5.0 Hz, 4H), 2.65 (s, 3H), 2.44 (d, *J* = 0.5 Hz, 3H), 1.90 (app t, *J* = 5.0 Hz, 4H).

3-Methyl-1-(6-methyl-2-(methylthio)pyrido[3,4-*d*]pyrimidin-8-yl)azetidine-3-carbonitrile **25**. Using 3-methylazetidine-3-carbonitrile hydrochloride. Yield = 66%. HRMS (ESI) *m/z* calcd for C₁₄H₁₆N₅S (M + H) 268.1121, found 268.1119; ¹H NMR (500 MHz, CD₃OD) δ 9.05 (s, 1H), 6.89 (app s, 1H), 4.83 (br d, *J* = 7.5 Hz, 2H), 4.48 (br d, *J* = 7.5 Hz, 2H), 2.64 (s, 3H), 2.47 (d, *J* = 0.5 Hz, 3H), 1.78 (s, 3H).

General Procedure for *m*-CPBA Oxidation on 23–25. To a cooled (0 °C) solution of appropriate sulfide (1 equiv) in CH₂Cl₂ (10 mL) was added *m*-CPBA (3 equiv). The reaction mixture was stirred for 18 h, while slowly warming to r.t. In some instances, further *m*-CPBA was needed to achieve full conversion. The reaction mixture was quenched with water and extracted with CH₂Cl₂. The combined organic layers were washed with aq. sat. NaHCO₃, dried (MgSO₄), and concentrated *in vacuo*. The residue was purified by flash column chromatography (0–10% MeOH in CH₂Cl₂).

2-(6-Methyl-2-(methylsulfonyl)pyrido[3,4-*d*]pyrimidin-8-yl)-7-oxa-2-azaspiro[3.5]nonane **27**. Using 2-(6-methyl-2-(methylthio)pyrido[3,4-*d*]pyrimidin-8-yl)-7-oxa-2-azaspiro[3.5]nonane **24**. Yield = 28%. HRMS (ESI) *m/z* calcd for C₁₆H₂₁N₄O₃S (M + H) 349.1329, found 349.1318; ¹H NMR (500 MHz, CD₃OD) δ 9.38 (s, 1H), 6.94 (s, 1H), 4.29 (br s, 4H), 3.73 (app t, *J* = 5.5 Hz, 4H), 3.43 (s, 3H), 2.53 (s, 3H), 1.92 (app t, *J* = 5.5 Hz, 4H).

3-Methyl-1-(6-methyl-2-(methylsulfonyl)pyrido[3,4-*d*]pyrimidin-8-yl)azetidine-3-carbonitrile **28**. Using 3-methyl-1-(6-methyl-2-(methylthio)pyrido[3,4-*d*]pyrimidin-8-yl)azetidine-3-carbonitrile **25**. Yield = 77%. HRMS (ESI) *m/z* calcd for C₁₄H₁₆N₅O₂S (M + H) 318.1019, found 318.1009; ¹H NMR (500 MHz, CD₃OD) δ 9.46 (s, 1H), 7.08 (s, 1H), 4.54 (br s, 4H), 3.44 (s, 3H), 2.56 (s, 3H), 1.80 (s, 3H).

*N*²-(4-(1,2-Dimethyl-1*H*-imidazol-5-yl)-2-methoxyphenyl)-6-methyl-*N*⁸-neopentylpyrido[3,4-*d*]pyrimidine-2,8-diamine **34**. To a cooled (0 °C) solution of *N*-(4-(1,2-dimethyl-1*H*-imidazol-5-yl)-2-methoxyphenyl)formamide **12** (17 mg, 0.069 mmol) in THF (3 mL) was added sodium hydride (2.7 mg, 0.11 mmol, 60% dispersion in oil). The reaction mixture was stirred at r.t. for 10 min. The reaction mixture was cooled to 0 °C, and 6-methyl-2-(methylsulfonyl)-*N*-neopentylpyrido[3,4-*d*]pyrimidin-8-amine **26**²⁸ (25.6 mg, 0.083 mmol) was added. The reaction mixture was stirred for 18 h, while slowly warming to r.t. aq NaOH (1 M, 1 mL) and MeOH (1 mL) were added, and the reaction mixture was stirred at r.t. for 1 h. The reaction mixture was concentrated *in vacuo*, and the residue diluted with EtOAc and water. The aqueous layer was re-extracted with EtOAc and CH₂Cl₂. The combined organic layers were washed with water and brine, dried (MgSO₄), and concentrated *in vacuo*. The residue was purified by flash column chromatography (0–10% MeOH in EtOAc) and followed by SCX-2 cartridge (MeOH, 1 M NH₃ in MeOH) to afford the title compound (3.3 mg, 11%). HRMS (ESI) *m/z* calcd for C₂₅H₃₂N₇O (M + H) 446.2663, found 446.2648; ¹H NMR (500 MHz, CD₃OD) δ 9.02 (s, 1H), 8.57 (d, *J* = 8.5 Hz, 1H), 7.09 (d, *J* = 2.0 Hz, 1H), 7.02 (dd, *J* = 8.5, 2.0 Hz, 1H), 6.88 (s, 1H), 6.70 (d, *J* = 1.0 Hz, 1H), 4.02 (s, 3H), 3.61 (s, 3H), 3.45 (s, 2H), 2.45 (s, 3H), 2.44 (d, *J* = 1.0 Hz, 3H), 1.09 (s, 9H).

General Procedure for Cesium Carbonate Mediated Substitution on 26, 27, or 28. To a solution of the appropriate sulfone (1 equiv) in DMSO (20 mg sulfone/mL) was added appropriate formamide (1.2 equiv) and cesium carbonate (2 equiv). The reaction mixture was heated to 120 °C in a closed cap vial for 18 h. The reaction mixture was diluted with EtOAc and water. The aqueous layer was re-extracted with EtOAc, and the combined organic layers were dried (MgSO₄) and concentrated *in vacuo*. The residue was purified by flash column chromatography (0–10% MeOH in CH₂Cl₂) and if necessary

followed by SCX-2 cartridge (MeOH, 1 M NH₃ in MeOH) to afford the title compounds.

*N*²-(2-Methoxy-4-(4-methyl-4H-1,2,4-triazol-3-yl)phenyl)-6-methyl-*N*⁸-neopentylpyrido[3,4-*d*]pyrimidine-2,8-diamine **35**. Using 6-methyl-2-(methylsulfonyl)-*N*-neopentylpyrido[3,4-*d*]pyrimidin-8-amine **26** and *N*-(2-methoxy-4-(4-methyl-4H-1,2,4-triazol-3-yl)phenyl)formamide **13**. Yield = 48%. HRMS (ESI) *m/z* calcd for C₂₃H₂₉N₈O (M + H) 433.2459, found 433.2447; ¹H NMR (500 MHz, CD₃OD) δ 9.05 (s, 1H), 8.75 (d, *J* = 8.5 Hz, 1H), 8.56 (s, 1H), 7.42 (d, *J* = 2.0 Hz, 1H), 7.34 (dd, *J* = 8.5, 2.0 Hz, 1H), 6.71 (d, *J* = 1.0 Hz, 1H), 4.07 (s, 3H), 3.87 (s, 3H), 3.48 (s, 2H), 2.44 (app s, 3H), 1.10 (s, 9H).

*N*²-(2-Ethoxy-4-(4-methyl-4H-1,2,4-triazol-3-yl)phenyl)-6-methyl-*N*⁸-neopentylpyrido[3,4-*d*]pyrimidine-2,8-diamine **36**. Using 6-methyl-2-(methylsulfonyl)-*N*-neopentylpyrido[3,4-*d*]pyrimidin-8-amine **26** and *N*-(2-ethoxy-4-(4-methyl-4H-1,2,4-triazol-3-yl)phenyl)formamide **29**. Yield = 70%. HRMS (ESI) *m/z* calcd for C₂₄H₃₁N₈O (M + H) 447.2615, found 447.2629; ¹H NMR (500 MHz, acetone-*d*₆) δ 9.11 (s, 1H), 8.80 (d, *J* = 8.5 Hz, 1H), 8.37 (s, 1H), 8.21 (br s, 1H), 7.46 (d, *J* = 2.0 Hz, 1H), 7.40 (dd, *J* = 8.5, 2.0 Hz, 1H), 6.74 (d, *J* = 0.5 Hz, 1H), 4.35 (q, *J* = 7.0 Hz, 2H), 3.90 (s, 3H), 3.51 (s, 2H), 2.41 (d, *J* = 0.5 Hz, 3H), 1.55 (t, *J* = 7.0 Hz, 3H), 1.08 (s, 9H).

*N*²-(4-(4,5-Dimethyl-4H-1,2,4-triazol-3-yl)-2-ethoxyphenyl)-6-methyl-*N*⁸-neopentylpyrido[3,4-*d*]pyrimidine-2,8-diamine **37**. Using 6-methyl-2-(methylsulfonyl)-*N*-neopentylpyrido[3,4-*d*]pyrimidin-8-amine **26**²⁸ and *N*-(2-ethoxy-4-(4,5-dimethyl-4H-1,2,4-triazol-3-yl)phenyl)formamide **30**. Yield = 56%. HRMS (ESI) *m/z* calcd for C₂₅H₃₃N₈O (M + H) 461.2772, found 461.2756; ¹H NMR (500 MHz, CD₃OD) δ 9.06 (s, 1H), 8.75 (d, *J* = 8.5 Hz, 1H), 7.34 (d, *J* = 1.9 Hz, 1H), 7.28 (dd, *J* = 8.5, 1.9 Hz, 1H), 6.72 (s, 1H), 4.30 (q, *J* = 7.2 Hz, 2H), 3.71 (s, 3H), 3.48 (s, 2H), 2.53 (s, 3H), 2.45 (s, 3H), 1.56 (t, *J* = 7.2 Hz, 3H), 1.10 (s, 9H).

*N*²-(4-(6,7-Dihydro-5H-pyrrolo[2,1-*c*][1,2,4]triazol-3-yl)-2-methoxyphenyl)-6-methyl-*N*⁸-neopentylpyrido[3,4-*d*]pyrimidine-2,8-diamine **38**. Using 6-methyl-2-(methylsulfonyl)-*N*-neopentylpyrido[3,4-*d*]pyrimidin-8-amine **26**²⁸ and *N*-(4-(6,7-dihydro-5H-pyrrolo[2,1-*c*][1,2,4]triazol-3-yl)-2-methoxyphenyl)formamide **31**. Purified by SCX-2 cartridge (MeOH, 1 M NH₃ in MeOH) followed by purification by HPLC. Yield = 31%. HRMS (ESI) *m/z* calcd for C₂₅H₃₁N₈O (M + H) 459.2615, found 459.2571; ¹H NMR (500 MHz, CDCl₃) δ 8.92 (s, 1H), 8.71 (d, *J* = 8.3 Hz, 1H), 8.07 (s, 1H), 7.66 (d, *J* = 1.9 Hz, 1H), 7.26 (br d, *J* = 1.9 Hz, 1H), 6.59 (d, *J* = 0.9 Hz, 1H), 6.53 (br t, *J* = 5.9 Hz, 1H), 4.24 (t, *J* = 6.9 Hz, 2H), 4.04 (s, 3H), 3.49 (d, *J* = 5.9 Hz, 2H), 3.06 (dd, *J* = 8.3, 6.9 Hz, 2H), 2.95–2.80 (m, 2H), 2.48 (d, *J* = 0.9 Hz, 3H), 1.11 (s, 9H).

*N*²-(4-(6,7-Dihydro-5H-pyrrolo[2,1-*c*][1,2,4]triazol-3-yl)-2-ethoxyphenyl)-6-methyl-*N*⁸-neopentylpyrido[3,4-*d*]pyrimidine-2,8-diamine **39**. Using 6-methyl-2-(methylsulfonyl)-*N*-neopentylpyrido[3,4-*d*]pyrimidin-8-amine **26**²⁸ and *N*-(4-(6,7-dihydro-5H-pyrrolo[2,1-*c*][1,2,4]triazol-3-yl)-2-ethoxyphenyl)formamide **32**. Yield = 35%. HRMS (ESI) *m/z* calcd for C₂₆H₃₃N₈O (M+H) 473.2777, found 473.2769; ¹H NMR (500 MHz, CD₃OD) δ 9.00 (s, 1H), 8.67 (d, *J* = 8.5 Hz, 1H), 7.51 (d, *J* = 1.8 Hz, 1H), 7.39 (dd, *J* = 8.5, 1.8 Hz, 1H), 6.67 (s, 1H), 4.35–4.28 (m, 4H), 3.47 (s, 2H), 3.04–3.01 (m, 2H), 2.91–2.87 (m, 2H), 2.43 (s, 3H), 1.57 (t, *J* = 6.9 Hz, 3H), 1.10 (s, 9H).

*N*²-(4-(5-(2-(Dimethylamino)ethyl)-4-methyl-4H-1,2,4-triazol-3-yl)-2-ethoxyphenyl)-6-methyl-*N*⁸-neopentylpyrido[3,4-*d*]pyrimidine-2,8-diamine **40**. Using 6-methyl-2-(methylsulfonyl)-*N*-neopentylpyrido[3,4-*d*]pyrimidin-8-amine **26**²⁸ and *N*-(4-(5-(2-(dimethylamino)ethyl)-4-methyl-4H-1,2,4-triazol-3-yl)-2-ethoxyphenyl)formamide **33**. Purified by reverse phase flash column chromatography (0–100% water in MeOH, followed by 0–30% 2 M methanolic ammonia in CH₂Cl₂). Yield = 18%. HRMS (ESI) *m/z* calcd for C₂₈H₄₀N₉O (M + H) 518.3356, found 518.3370; ¹H NMR (500 MHz, CD₃OD) δ 9.05 (s, 1H), 8.75 (d, *J* = 8.5 Hz, 1H), 7.34 (d, *J* = 1.8 Hz, 1H), 7.28 (dd, *J* = 8.5, 1.8 Hz, 1H), 6.71 (s, 1H), 4.30 (q, *J* = 7.0 Hz, 2H), 3.73 (s, 3H), 3.47 (s, 2H), 3.09 (app t, *J* = 7.5 Hz, 2H), 2.91 (app t, *J* = 7.5 Hz, 2H), 2.44 (s, 3H), 2.42 (s, 6H), 1.56 (t, *J* = 7.0 Hz, 3H), 1.09 (s, 9H).

N-(2-Ethoxy-4-(4-methyl-4H-1,2,4-triazol-3-yl)phenyl)-6-methyl-8-(7-oxa-2-azaspiro[3.5]nonan-2-yl)pyrido[3,4-*d*]pyrimidin-2-amine **41**. Using 2-(6-methyl-2-(methylsulfonyl)pyrido[3,4-*d*]pyrimidin-8-yl)-7-oxa-2-azaspiro[3.5]nonane **27** and *N*-(2-ethoxy-4-(4-methyl-4H-1,2,4-triazol-3-yl)phenyl)formamide **29**. Yield = 46%. HRMS (ESI) *m/z* calcd for C₂₆H₃₁N₈O₂ (M + H) 487.2564, found 487.2511; ¹H NMR (500 MHz, CD₃OD) δ 9.06 (s, 1H), 8.57 (d, *J* = 8.5 Hz, 1H), 8.56 (s, 1H), 7.39 (d, *J* = 2.0 Hz, 1H), 7.36 (dd, *J* = 8.5, 2.0 Hz, 1H), 6.78 (s, 1H), 4.31–4.27 (m, 6H), 3.87 (s, 3H), 3.69 (app t, *J* = 5.5 Hz, 4H), 2.44 (s, 3H), 1.89 (app t, *J* = 5.5 Hz, 4H), 1.54 (t, *J* = 7.0 Hz, 3H).

1-(2-((2-Ethoxy-4-(4-methyl-4H-1,2,4-triazol-3-yl)phenyl)-amino)-6-methylpyrido[3,4-*d*]pyrimidin-8-yl)-3-methylazetidine-3-carbonitrile **42**. Using 3-methyl-1-(6-methyl-2-(methylsulfonyl)pyrido[3,4-*d*]pyrimidin-8-yl)azetidine-3-carbonitrile **28** and *N*-(2-ethoxy-4-(4-methyl-4H-1,2,4-triazol-3-yl)phenyl)formamide **29**. Yield = 38%. HRMS (ESI) *m/z* calcd for C₂₄H₂₆N₉O (M + H) 456.2255, found 456.2180; ¹H NMR (500 MHz, CD₃OD) δ 9.10 (s, 1H), 8.56 (s, 1H), 8.46 (d, *J* = 8.5 Hz, 1H), 7.40 (dd, *J* = 8.5, 2.0 Hz, 1H), 7.39 (d, *J* = 2.0 Hz, 1H), 6.91 (s, 1H), 4.75 (d, *J* = 9.0 Hz, 2H), 4.39 (d, *J* = 9.0 Hz, 2H), 4.28 (q, *J* = 7.0 Hz, 2H), 3.88 (s, 3H), 2.47 (s, 3H), 1.75 (s, 3H), 1.53 (t, *J* = 7.0 Hz, 3H).

Preparation of Compounds in Scheme 3. 8-Chloro-6-methyl-2-(methylsulfonyl)pyrido[3,4-*d*]pyrimidine **43**. A suspension of 8-chloro-6-methyl-2-(methylthio)pyrido[3,4-*d*]pyrimidine **22** (1.13 g, 5.01 mmol) in CH₂Cl₂ (50 mL) was treated with *m*-CPBA (77% w/w, 2.60 g, 11.57 mmol) at 0 °C. The reaction mixture was stirred for 18 h, while slowly warming to r.t. The reaction was quenched with water and extracted with CH₂Cl₂. The combined organic layers were washed with aq. sat. NaHCO₃, dried (MgSO₄), and concentrated *in vacuo*. The residue was purified by flash column chromatography (0–70% EtOAc in cyclohexane) to afford the title compound (972 mg, 75%). HRMS (ESI) *m/z* calcd for C₉H₉ClN₃O₂S (M + H) 258.0099, found 258.0092; ¹H NMR (500 MHz, CD₃OD) δ 9.82 (s, 1H), 7.96 (d, *J* = 0.5 Hz, 1H), 3.54 (s, 3H), 2.78 (d, *J* = 0.5 Hz, 3H).

8-Chloro-*N*-(2-ethoxy-4-(4-methyl-4H-1,2,4-triazol-3-yl)phenyl)-6-methylpyrido[3,4-*d*]pyrimidin-2-amine **44**. To a solution of *N*-(2-ethoxy-4-(4-methyl-4H-1,2,4-triazol-3-yl)phenyl)formamide **29** (1.88 g, 7.63 mmol) in THF (70 mL) was added NaH (60% w/w, 500 mg, 12.50 mmol) at 0 °C. The reaction mixture was stirred at r.t. for 30 min. The mixture was cooled to 0 °C, and 8-chloro-6-methyl-2-(methylsulfonyl)pyrido[3,4-*d*]pyrimidine **43** (2.50 g, 9.70 mmol) was added. The reaction mixture was stirred for 18 h, while slowly warming to r.t. aq. NaOH (2 M, 25 mL) and MeOH (25 mL) were added, and the resulting mixture stirred at r.t. for 1 h. The reaction mixture was concentrated *in vacuo*, and the residue was diluted with CH₂Cl₂ and water. The aqueous layer was extracted with CH₂Cl₂, and the combined organic layers were dried (MgSO₄) and concentrated *in vacuo*. The residue was purified by flash column chromatography (0–6% MeOH in CH₂Cl₂) to afford the title compound (3.24 g, quant). HRMS (ESI) *m/z* calcd for C₁₉H₁₉ClN₅O (M + H) 396.1339, found 396.1335; ¹H NMR (500 MHz, (CD₃)₂SO) δ 9.46 (s, 1H), 8.85 (d, *J* = 8.3 Hz, 1H), 8.79 (s, 1H), 8.56 (s, 1H), 7.74 (d, *J* = 1.0 Hz, 1H), 7.49–7.36 (m, 2H), 4.25 (q, *J* = 7.0 Hz, 2H), 3.80 (s, 3H), 2.58 (s, 3H), 1.43 (t, *J* = 7.0 Hz, 3H).

General Procedure for Amine Displacement on 44 (Compounds 45–48). To a solution of the appropriate chloro compound (1 equiv) in NMP (3 mL) was added the appropriate amine or salt thereof (2–5 equiv) and triethylamine (5 equiv). The reaction mixture was heated to 100 °C in a closed cap vial for 18 h. The reaction mixture was diluted with EtOAc and water. The organic layer was washed with brine, dried (MgSO₄), and concentrated *in vacuo*. The residue was purified by flash column chromatography (eluting with the appropriate solvent system) and, if necessary, followed by SCX-2 cartridge (MeOH, 1 M NH₃ in MeOH).

(*S*)-*N*⁸-(3,3-Dimethylbutan-2-yl)-*N*²-(2-ethoxy-4-(4-methyl-4H-1,2,4-triazol-3-yl)phenyl)-6-methylpyrido[3,4-*d*]pyrimidine-2,8-diamine **45**. Using 8-chloro-*N*-(2-ethoxy-4-(4-methyl-4H-1,2,4-triazol-3-yl)phenyl)-6-methylpyrido[3,4-*d*]pyrimidin-2-amine **44** and (*S*)-3,3-dimethylbutan-2-amine at 130 °C for 2 days. Yield = 52%. HRMS (ESI) *m/z* calcd for C₂₅H₃₃N₈O (M + H) 461.2777, found 461.2777;

^1H NMR (500 MHz, $(\text{CD}_3)_2\text{SO}$) δ 9.15 (s, 1H), 8.57 (s, 1H), 8.43 (d, $J = 8.3$ Hz, 1H), 7.41 (d, $J = 1.9$ Hz, 1H), 7.31 (dd, $J = 8.2, 1.9$ Hz, 1H), 6.72 (d, $J = 1.0$ Hz, 1H), 6.43 (d, $J = 9.5$ Hz, 1H), 4.23 (q, $J = 6.9$ Hz, 2H), 4.13 (dq, $J = 9.4, 6.6$ Hz, 1H), 3.78 (s, 3H), 2.38 (s, 3H), 1.41 (t, $J = 6.9$ Hz, 3H), 1.16 (d, $J = 6.6$ Hz, 3H), 1.00 (s, 9H).

N-(2-Ethoxy-4-(4-methyl-4H-1,2,4-triazol-3-yl)phenyl)-6-methyl-8-(pyrrolidin-1-yl)pyrido[3,4-*d*]pyrimidin-2-amine **46**. Using 8-chloro-*N*-(2-ethoxy-4-(4-methyl-4H-1,2,4-triazol-3-yl)phenyl)-6-methylpyrido[3,4-*d*]pyrimidin-2-amine **44** and pyrrolidine at 130 °C. Yield = 70%. HRMS (ESI) m/z calcd for $\text{C}_{23}\text{H}_{27}\text{N}_8\text{O}$ ($\text{M} + \text{H}$) 431.2308, found 431.2315; ^1H NMR (500 MHz, $(\text{CD}_3)_2\text{SO}$) δ 9.13 (s, 1H), 8.56 (s, 1H), 8.34 (s, 1H), 8.23 (d, $J = 8.2$ Hz, 1H), 7.39–7.29 (m, 2H), 6.76 (d, $J = 0.8$ Hz, 1H), 4.21 (q, $J = 6.9$ Hz, 2H), 3.88 (s, 4H), 3.78 (s, 3H), 2.37 (s, 3H), 1.94–1.83 (m, 4H), 1.41 (t, $J = 6.9$ Hz, 3H).

8-(3,3-Dimethylazetididin-1-yl)-*N*-(2-ethoxy-4-(4-methyl-4H-1,2,4-triazol-3-yl)phenyl)-6-methylpyrido[3,4-*d*]pyrimidin-2-amine **47**. Using 8-chloro-*N*-(2-ethoxy-4-(4-methyl-4H-1,2,4-triazol-3-yl)phenyl)-6-methylpyrido[3,4-*d*]pyrimidin-2-amine **44** and 3,3-dimethylazetididine hydrochloride. Yield = 70%. HRMS (ESI) m/z calcd for $\text{C}_{24}\text{H}_{30}\text{N}_8\text{O}$ ($\text{M} + 2\text{H}$)/2 223.1266, found 223.1261; ^1H NMR (500 MHz, CD_3OD) δ 9.05 (s, 1H), 8.56 (d, $J = 8.5$ Hz, 1H), 8.54 (s, 1H), 7.37 (d, $J = 1.5$ Hz, 1H), 7.34 (dd, $J = 8.5, 1.5$ Hz, 1H), 6.77 (s, 1H), 4.29 (q, $J = 7.0$ Hz, 2H), 4.21 (br s, 4H), 3.87 (s, 3H), 2.44 (s, 3H), 1.54 (t, $J = 7.0$ Hz, 3H), 1.38 (s, 6H).

8-(2,2-Dimethylazetididin-1-yl)-*N*-(2-ethoxy-4-(4-methyl-4H-1,2,4-triazol-3-yl)phenyl)-6-methylpyrido[3,4-*d*]pyrimidin-2-amine **48**. Using 8-chloro-*N*-(2-ethoxy-4-(4-methyl-4H-1,2,4-triazol-3-yl)phenyl)-6-methylpyrido[3,4-*d*]pyrimidin-2-amine **44** and 2,2-dimethylazetididine. Yield = 89%. HRMS (ESI) m/z calcd for $\text{C}_{24}\text{H}_{29}\text{N}_8\text{O}$ ($\text{M} + \text{H}$) 445.2459, found 445.2461; ^1H NMR (500 MHz, CD_3OD) δ 8.98 (s, 1H), 8.54 (s, 1H), 8.52 (d, $J = 8.0$ Hz, 1H), 7.35 (d, $J = 2.0$ Hz, 1H), 7.33 (dd, $J = 8.0, 2.0$ Hz, 1H), 6.65 (s, 1H), 4.70–4.66 (m, 2H), 4.27 (d, $J = 7.0$ Hz, 2H), 3.85 (s, 3H), 2.39 (s, 3H), 2.22 (dd, $J = 9.0, 7.5$ Hz, 2H), 1.71 (s, 6H), 1.54 (t, $J = 7.0$ Hz, 3H).

Biochemical Assays. MPS1 and CDK2 counterscreen assay were performed as reported previously.¹⁶

MSD Assay. An electrochemiluminescence assay (Meso Scale Discovery, MSD) for detection of autophosphorylation of MPS1 at pTpS^{33/37} sites in cell lysates has been described previously.¹⁶ Autophosphorylation of MPS1 at pTpS^{33/37} and total MPS1-GFP levels in MPS1-doxycycline inducible DLD-1 xenografts were determined by MSD assays as described previously.³² Results were presented as the ratio of Phospho-MPS1/Total MPS1.

Microsomal Metabolism. Microsomal clearance was determined in female CD1 mice, female Sprague–Dawley rats, and mixed gender human liver microsomes obtained from Tebu-Bio (Peterborough, U.K.) following incubation of 1 μM compound at 37 °C in 1 mg/mL microsomal protein, 3 mmol/L MgCl_2 , 1 mmol/L NADPH, 2.5 mmol/L UDP-glucuronic acid, and 10 mmol/L phosphate buffer (pH 7.4) (all purchased from Sigma-Aldrich, Gillingham, U.K.). Reactions were started by addition of the cofactors following 10 min preincubation of microsomes with test compound and were terminated at –1, 0, 5, 10, 15, and 30 min with three volumes of ice-cold methanol containing internal standard. Samples were centrifuged at 2800g for 30 min at 4 °C and the supernatants analyzed. Control incubations were prepared as above with omission of cofactors. Compound measurements were performed by LCMS on an Agilent quadrupole time-of-flight instrument (Agilent 6510) following separation with a 6 min gradient of 0.1% formic acid in methanol on a 50 \times 2.1 mm 2.6 μm C18 column (Kinetex Phenomenex). For metabolite identification, the gradient was extended to 20 min and MS/MS carried out with fragment elucidation for ions of interest.

Pharmacokinetic Studies. Animals were adapted to laboratory conditions for at least 1 week prior to dosing and were allowed food and water *ad libitum*. Compounds were administered iv or po (mouse, 0.1 mL/10 g in 10% DMSO, 5% tween 20 in saline; rat, 0.05 mL/10 g in 10% DMSO, 5% tween 20 in saline; dog, 10% in DMSO in saline). Blood samples were collected from the tail vein (20 μL) at 8 time

points over the 24 h post dose and spotted on Whatman B cards (VWR) together with a standard curve and quality controls spiked in control blood. Cards were allowed to dry at r.t. for at least 6 h. Cards were punched and 6 mm discs were extracted with 200 μL of methanol containing 500 nM olomoucine as an internal standard. Following centrifugation, extracts were analyzed by multiple reaction monitoring of precursor and product ions by ESI-LCMS/MS on a QTRAP 4000 (ABSciex) following gradient separation with 0.1% formic acid in methanol on a Phenomenex Kinetex C18 UPLC column (50 \times 2.1 mm, 2.6 μm). Quantitation was carried out with an external calibration (typically 8 points ranging from 1 nM to 25 μM). Quality controls were included (three concentrations) at the beginning and the end of the analytical run and were within 20% of nominal concentrations.

Pharmacokinetic parameters were derived from noncompartmental analysis using Phoenix Pharsight WinNonlin (model 200 and 201) version 6.1/6.3.

All experiments using animals were performed in accordance with the local Animal Welfare and Ethical Review Board, the UK Home Office Animals Scientific Procedures Act 1986, and with the United Kingdom National Cancer Research Institute Guidelines for the Welfare of Animals in Cancer Research.³¹ The ICR does not undertake research in nonrodent species and requires internal ethical review when such studies are sponsored by organizations with whom we collaborate. Collaborator-sponsored nonrodent pharmacology studies of compound **36** necessary for the prediction of therapeutic window and application to the clinic were approved by the ICR Animal Welfare and Ethics Review Board and were conducted in full compliance with national regulations at AAALAC accredited R&D sites.

PK/PD Experiments. These experiments were conducted as previously described.³²

■ ASSOCIATED CONTENT

Supporting Information

The Supporting Information is available free of charge on the ACS Publications website at DOI: 10.1021/acs.jmedchem.8b00690.

Molecular formula strings (CSV)

Experimental procedures and analytical data for all formamides (**10–13** and **29–33**) and corresponding intermediates, CYP, hERG activity, and P-gp efflux data as well as kinase selectivity profiling of **36**. Tables with standard deviations for all compounds as well as antiproliferative (GI_{50}) data for several compounds (PDF)

Accession Codes

The PDB ID code for **36** bound to MPS1 is 6H3K.

■ AUTHOR INFORMATION

Corresponding Author

*Tel: +44 (0)20 8722 4353. E-mail: swen.hoelder@icr.ac.uk.

ORCID

Julian Blagg: 0000-0002-7409-0323

Swen Hoelder: 0000-0001-8636-1488

Present Address

¹(A.F.) SBA School of Science and Engineering, Lahore University of Management Sciences, D.H.A., Lahore 54792, Pakistan.

Notes

The authors declare the following competing financial interest(s): The authors are current or former employees of The Institute of Cancer Research, which has a commercial interest in the development of kinase inhibitors.

ACKNOWLEDGMENTS

This work was supported by Cancer Research UK [grant number C309/A11566]. We also acknowledge the Cancer Research Technology Pioneer Fund and Sixth Element Capital for funding (to P.I.) and NHS funding to the NIHR Biomedical Research Centre. S.L. is also supported by Breakthrough Breast Cancer. We thank Dr. Amin Mirza, Dr. Maggie Liu, and Mr. Meirion Richards for their help with LC, NMR, and mass spectrometry. We are grateful to the staff of DIAMOND Light Source for their support during data collection.

ABBREVIATIONS USED

CDK2, cyclin-dependent kinase 2; Cl, clearance; hERG, human Ether-à-go-go-Related Gene; HLM, human liver microsomes; L.E., ligand efficiency; MLM, mouse liver microsomes; MPS, monopolar spindle kinase; MSD, Meso-Scale Discovery; MTT, 3-(4,5-dimethylthiazol-2-yl)-2,5-diphenyltetrazolium bromide; PARP, poly ADP ribose polymerase; PLK1, polo-like kinase; PTEN, phosphatase and tensin homologue; SAC, spindle assembly checkpoint; RLM, rat liver microsomes; V_{ss} , volume of distribution

REFERENCES

- (1) Hardwick, K. G. The spindle checkpoint. *Trends Genet.* **1998**, *14*, 1–4.
- (2) Mills, G. B.; Schmandt, R.; McGill, M.; Amendola, A.; Hill, M.; Jacobs, K.; May, C.; Rodricks, A. M.; Campbell, S.; Hogg, D. Expression of TTK, a novel human protein kinase, is associated with cell proliferation. *J. Biol. Chem.* **1992**, *267*, 16000–16006.
- (3) Lauze, E.; Stoelcker, B.; Luca, F. C.; Weiss, E.; Schutz, A. R.; Winey, M. Yeast spindle pole body duplication gene MPS1 encodes an essential dual specificity protein kinase. *EMBO J.* **1995**, *14*, 1655–1663.
- (4) Musacchio, A.; Salmon, E. D. The spindle-assembly checkpoint in space and time. *Nat. Rev. Mol. Cell Biol.* **2007**, *8*, 379–393.
- (5) Daniel, J.; Coulter, J.; Woo, J.-H.; Wilsbach, K.; Gabrielson, E. High levels of the MPS1 checkpoint protein are protective of aneuploidy in breast cancer cells. *Proc. Natl. Acad. Sci. U. S. A.* **2011**, *108*, 5384–5389.
- (6) Brough, R.; Frankum, J. R.; Sims, D.; Mackay, A.; Mendes-Pereira, A. M.; Bajrami, I.; Costa-Cabral, S.; Rafiq, R.; Ahmad, A. S.; Cerone, M. A.; Natrajan, R.; Sharpe, R.; Shiu, K.-K.; Wetterskog, D.; Dedes, K. J.; Lambros, M. B.; Rawjee, T.; Linardopoulos, S.; Reis-Filho, J. S.; Turner, N. C.; Lord, C. J.; Ashworth, A. Functional viability profiles of breast cancer. *Cancer Discovery* **2011**, *1*, 260–273.
- (7) Gordon, D. J.; Resio, B.; Pellman, D. Causes and consequences of aneuploidy in cancer. *Nat. Rev. Genet.* **2012**, *13*, 189–203.
- (8) Lengauer, C.; Kinzler, K. W.; Vogelstein, B. Genetic instabilities in human cancers. *Nature* **1998**, *396*, 643–649.
- (9) Carter, S. L.; Eklund, A. C.; Kohane, I. S.; Harris, L. N.; Szallasi, Z. A signature of chromosomal instability inferred from gene expression profiles predicts clinical outcome in multiple human cancers. *Nat. Genet.* **2006**, *38*, 1043–1048.
- (10) Yuan, B.; Xu, Y.; Woo, J.-H.; Wang, Y.; Bae, Y. K.; Yoon, D.-S.; Wersto, R. P.; Tully, E.; Wilsbach, K.; Gabrielson, E. Increased expression of mitotic checkpoint genes in breast cancer cells with chromosomal instability. *Clin. Cancer Res.* **2006**, *12*, 405–410.
- (11) Mizukami, Y.; Kono, K.; Daigo, Y.; Takano, A.; Tsunoda, T.; Kawaguchi, Y.; Nakamura, Y.; Fujii, H. Detection of novel cancer-testis antigen-specific T-cell responses in TIL, regional lymph nodes, and PBL in patients with esophageal squamous cell carcinoma. *Cancer Sci.* **2008**, *99*, 1448–1454.
- (12) Salvatore, G.; Nappi, T. C.; Salerno, P.; Jiang, Y.; Garbi, C.; Ugolini, C.; Miccoli, P.; Basolo, F.; Castellone, M. D.; Cirafici, A. M.; Melillo, R. M.; Fusco, A.; Bittner, M. L.; Santoro, M. A cell

proliferation and chromosomal instability signature in anaplastic thyroid carcinoma. *Cancer Res.* **2007**, *67*, 10148–10158.

- (13) Thykjaer, T.; Workman, C.; Kruhoffer, M.; Demtröder, K.; Wolf, H.; Andersen, L. D.; Frederiksen, C. M.; Knudsen, S.; Ørntoft, T. F. Identification of gene expression patterns in superficial and invasive human bladder cancer. *Cancer Res.* **2001**, *61*, 2492–2499.

- (14) Wengner, A. M.; Siemeister, G.; Koppitz, M.; Schulze, V.; Kosmund, D.; Klar, U.; Stoeckigt, D.; Neuhaus, R.; Lienau, P.; Bader, B.; Prechtel, S.; Raschke, M.; Frisk, A.-L.; von Ahnen, O.; Michels, M.; Kreft, B.; von Nussbaum, F.; Brands, M.; Mumberg, D.; Ziegelbauer, K. Novel MPS1 kinase inhibitors with potent antitumor activity. *Mol. Cancer Ther.* **2016**, *15*, 583–592.

- (15) Mason, J. M.; Wei, X.; Fletcher, G. C.; Kiarash, R.; Brox, R.; Hodgson, R.; Beletskaya, I.; Bray, M. R.; Mak, T. W. Functional characterization of CFI-402257, a potent and selective MPS1/TTK kinase inhibitor, for the treatment of cancer. *Proc. Natl. Acad. Sci. U. S. A.* **2017**, *114*, 3127–3132.

- (16) Naud, S.; Westwood, I. M.; Faisal, A.; Sheldrake, P.; Bavetsias, V.; Atrash, B.; Cheung, K.-M. J.; Liu, M.; Hayes, A.; Schmitt, J.; Wood, A.; Choi, V.; Boxall, K.; Mak, G.; Guden, M.; Valenti, M.; de Haven Brandon, A.; Henley, A.; Baker, R.; McAndrew, C.; Matijssen, B.; Burke, R.; Hoelder, S.; Eccles, S. A.; Raynaud, F. I.; Linardopoulos, S.; van Montfort, R. L. M.; Blagg, J. Structure-based design of orally bioavailable 1*H*-pyrrolo[3,2-*c*]pyridine inhibitors of mitotic kinase monopolar spindle 1 (MPS1). *J. Med. Chem.* **2013**, *56*, 10045–10065.

- (17) Innocenti, P.; Woodward, H. L.; Solanki, S.; Naud, S.; Westwood, I. M.; Cronin, N.; Hayes, A.; Roberts, J.; Henley, A. T.; Baker, R.; Faisal, A.; Mak, G. W.-Y.; Box, G.; Valenti, M.; De Haven Brandon, A.; O'Fee, L.; Saville, H.; Schmitt, J.; Matijssen, B.; Burke, R.; van Montfort, R. L. M.; Raynaud, F. I.; Eccles, S. A.; Linardopoulos, S.; Blagg, J.; Hoelder, S. Rapid discovery of pyrido[3,4-*d*]pyrimidine inhibitors of monopolar spindle kinase 1 (MPS1) using a structure-based hybridization approach. *J. Med. Chem.* **2016**, *59*, 3671–3688.

- (18) Tardif, K. D.; Rogers, A.; Cassiano, J.; Roth, B. L.; Cimbor, D. M.; McKinnon, R.; Peterson, A.; Douce, T. B.; Robinson, R.; Dorweiler, I.; Davis, T.; Hess, M. A.; Ostanin, K.; Papac, D. I.; Baichwal, V.; McAlexander, I.; Willardson, J. A.; Saunders, M.; Christophe, H.; Kumar, D. V.; Wettstein, D. A.; Carlson, R. O.; Williams, B. L. Characterization of the cellular and antitumor effects of MPI-0479605, a small-molecule inhibitor of the mitotic kinase MPS1. *Mol. Cancer Ther.* **2011**, *10*, 2267–2275.

- (19) Tannous, B. A.; Kerami, M.; Van der Stoop, P. M.; Kwiatkowski, N.; Wang, J.; Zhou, W.; Kessler, A. F.; Lewandrowski, G.; Hiddingh, L.; Sol, N.; Lagerweij, T.; Wedekind, L.; Niers, J. M.; Barazas, M.; Nilsson, R. J. A.; Geerts, D.; De Witt Hamer, P. C.; Hagemann, C.; Vandertop, W. P.; Van Tellingen, O.; Noske, D. P.; Gray, N. S.; Würdinger, T. Effects of the selective MPS1 inhibitor MPS1-IN-3 on glioblastoma sensitivity to antimitotic drugs. *J. Natl. Canc. Inst.* **2013**, *105*, 1322–1331.

- (20) Kusakabe, K.-I.; Ide, N.; Daigo, Y.; Itoh, T.; Yamamoto, T.; Kojima, E.; Mitsuoka, Y.; Tadano, G.; Tagashira, S.; Higashino, K.; Okano, Y.; Sato, Y.; Inoue, M.; Iguchi, M.; Kanazawa, T.; Ishioka, Y.; Dohi, K.; Kido, Y.; Sakamoto, S.; Ando, S.; Maeda, M.; Higaki, M.; Yoshizawa, H.; Murai, H.; Nakamura, Y. A unique hinge binder of extremely selective aminopyridine-based MPS1 (TTK) kinase inhibitors with cellular activity. *Bioorg. Med. Chem.* **2015**, *23*, 2247–2260.

- (21) Laufer, R.; Ng, G.; Liu, Y.; Patel, N. K. B.; Edwards, L. G.; Lang, Y.; Li, S.-W.; Feher, M.; Awrey, D. E.; Leung, G.; Beletskaya, I.; Plotnikova, O.; Mason, J. M.; Hodgson, R.; Wei, X.; Mao, G.; Luo, X.; Huang, P.; Green, E.; Kiarash, R.; Lin, D. C.-C.; Harris-Brandts, M.; Ban, F.; Nadeem, V.; Mak, T. W.; Pan, G. J.; Qiu, W.; Chirgadze, N. Y.; Pauls, H. W. Discovery of inhibitors of the mitotic kinase TTK based on *N*-(3-(3-sulfamoylphenyl)-1*H*-indazol-5-yl)-acetamides and carboxamides. *Bioorg. Med. Chem.* **2014**, *22*, 4968–4997.

- (22) Martinez, R.; Blasina, A.; Hallin, J. F.; Hu, W.; Rymer, I.; Fan, J.; Hoffman, R. L.; Murphy, S.; Marx, M.; Yanocho, G.; Trajkovic, D.; Dinh, D.; Timofeevski, S.; Zhu, Z.; Sun, P.; Lappin, P. B.; Murray,

B. W. Mitotic checkpoint kinase MPS1 has a role in normal physiology which impacts clinical utility. *PLoS One* **2015**, *10*, e0138616.

(23) Maia, A. R. R.; de Man, J.; Boon, U.; Janssen, A.; Song, J. Y.; Omerzu, M.; Sterrenburg, J. G.; Prinsen, M. B. W.; Willemsen-Seegers, N.; de Roos, J. A. D. M.; van Doornmalen, A. M.; Uitdehaag, J. C. M.; Kops, G. J. P. L.; Jonkers, J.; Buijsman, R. C.; Zaman, G. J. R.; Medema, R. H. Inhibition of the spindle assembly checkpoint kinase TTK enhances the efficacy of docetaxel in a triple-negative breast cancer model. *Ann. Oncol.* **2015**, *26*, 2180–2192.

(24) Wengner, A. M.; Siemeister, G. Combinations for the Treatment of Cancer Comprising a MPS-1 Kinase Inhibitor and a Mitotic Inhibitor. WO2014198645, 2014.

(25) Wengner, A. M.; Siemeister, G. Combination of a Imidazopyridazine Derivative and a Mitotic Agent for the Treatment of Cancer. WO2014198776A1, 2014.

(26) Kusakabe, K.-I.; Ide, N.; Daigo, Y.; Itoh, T.; Yamamoto, T.; Hashizume, H.; Nozu, K.; Yoshida, H.; Tadano, G.; Tagashira, S.; Higashino, K.; Okano, Y.; Sato, Y.; Inoue, M.; Iguchi, M.; Kanazawa, T.; Ishioka, Y.; Dohi, K.; Kido, Y.; Sakamoto, S.; Ando, S.; Maeda, M.; Higaki, M.; Baba, Y.; Nakamura, Y. Discovery of imidazo[1,2-*b*]pyridazine derivatives: selective and orally available MPS1 (TTK) kinase inhibitors exhibiting remarkable antiproliferative activity. *J. Med. Chem.* **2015**, *58*, 1760–1775.

(27) Wahba, H. A.; El-Hadaad, H. A. Current approaches in treatment of triple-negative breast cancer. *Cancer Biol. Med.* **2015**, *12*, 106–116.

(28) Innocenti, P.; Woodward, H.; O'Fee, L.; Hoelder, S. Expanding the scope of fused pyrimidines as kinase inhibitor scaffolds: synthesis and modification of pyrido[3,4-*d*]pyrimidines. *Org. Biomol. Chem.* **2015**, *13*, 893–904.

(29) VanderWel, S. N.; Harvey, P. J.; McNamara, D. J.; Repine, J. T.; Keller, P. R.; Quin, J.; Booth, R. J.; Elliott, W. L.; Dobrusin, E. M.; Fry, D. W.; Toogood, P. L. Pyrido[2,3-*d*]pyrimidin-7-ones as specific inhibitors of cyclin-dependent kinase 4. *J. Med. Chem.* **2005**, *48*, 2371–2387.

(30) Toogood, P. L.; Harvey, P. J.; Repine, J. T.; Sheehan, D. J.; VanderWel, S. N.; Zhou, H.; Keller, P. R.; McNamara, D. J.; Sherry, D.; Zhu, T.; Brodfuehrer, J.; Choi, C.; Barvian, M. R.; Fry, D. W. Discovery of a potent and selective inhibitor of cyclin-dependent kinase 4/6. *J. Med. Chem.* **2005**, *48*, 2388–2406.

(31) Workman, P.; Aboagye, E. O.; Balkwill, F.; Balmain, A.; Bruder, G.; Chaplin, D. J.; Double, J. A.; Everitt, J.; Farningham, D. A. H.; Glennie, M. J.; Kelland, L. R.; Robinson, V.; Stratford, I. J.; Tozer, G. M.; Watson, S.; Wedge, S. R.; Eccles, S. A. Guidelines for the welfare and use of animals in cancer research. *Br. J. Cancer* **2010**, *102*, 1555–1577.

(32) Faisal, A.; Mak, G. W. Y.; Gurden, M. D.; Xavier, C. P. R.; Anderhub, S. J.; Innocenti, P.; Westwood, I. M.; Naud, S.; Hayes, A.; Box, G.; Valenti, M. R.; De Haven Brandon, A. K.; O'Fee, L.; Schmitt, J.; Woodward, H. L.; Burke, R.; vanMontfort, R. L. M.; Blagg, J.; Raynaud, F. I.; Eccles, S. A.; Hoelder, S.; Linardopoulos, S. Characterisation of CCT271850, a selective, oral and potent MPS1 inhibitor, used to directly measure *in vivo* MPS1 inhibition vs therapeutic efficacy. *Br. J. Cancer* **2017**, *116*, 1166–1176.

(33) Milletti, F.; Storchi, L.; Sforna, G.; Cruciani, G. New and original pka prediction method using grid molecular interaction fields. *J. Chem. Inf. Model.* **2007**, *47*, 2172–2181.